Cell Reports

Article

Centrosome-dependent microtubule modifications set the conditions for axon formation

Graphical abstract

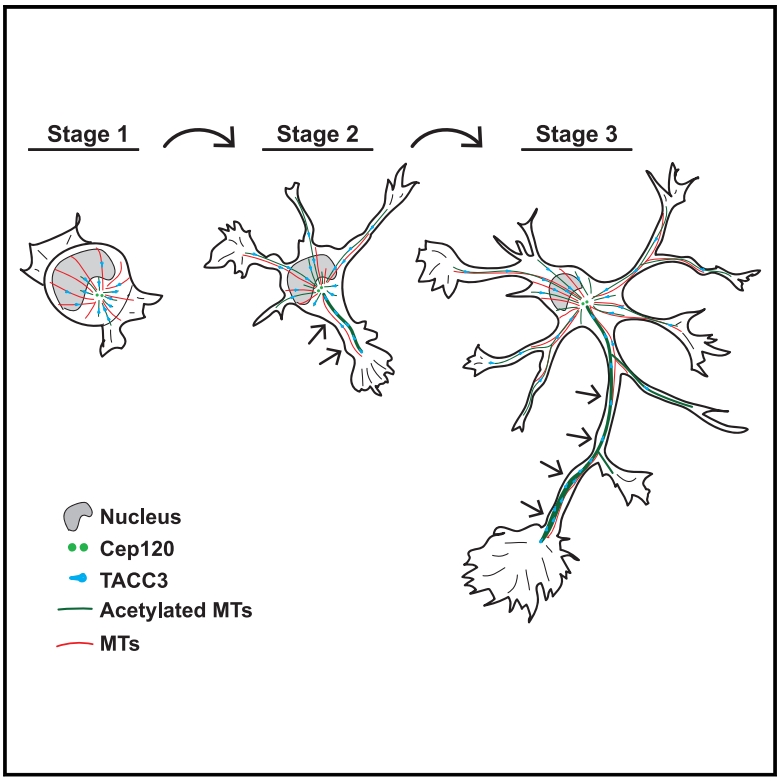

Highlights

- MT acetylation near the MTOC from stage 1 cells spread out to growing axons (stage 3)
- MT acetylation in soma at stage 1 is significantly lower compared with stage 2 neurons
- Centrosomal protein, Cep120, modulates axon formation through MT acetylation
- TACC3, an MT-stabilizing protein, is enriched in the longest neurites at stages 2 and 3

Authors

Durga Praveen Meka, Oliver Kobler, Shuai Hong, ..., Hartmut Schlüter, Eugenio F. Fornasiero, Froylan Calderon de Anda

Correspondence

froylan.calderon@zmnh.uni-hamburg.de

In brief

Meka et al. show that Cep120-dependent microtubule acetylation, concentrated at the centrosome at stage 1, spreads from the soma into neurites at stage 2 and is eventually enriched in the longest neurite (axon) at stage 3. Other tubulin modifications (polyglutamylation, tyrosination) or α-tubulin itself did not follow the gradual distribution during symmetry breakage.

Meka et al., 2022, Cell Reports *39*, 110686
April 19, 2022 © 2022 The Author(s).
https://doi.org/10.1016/j.celrep.2022.110686

CellPress

Cell Reports

CellPress
OPEN ACCESS

Article

Centrosome-dependent microtubule modifications set the conditions for axon formation

Durga Praveen Meka,[1] Oliver Kobler,[2,9] Shuai Hong,[1,9] Carina Meta Friedrich,[1,9] Souhaila Wuesthoff,[1] Melad Henis,[1,3] Birgit Schwanke,[1] Christoph Krisp,[4] Nessa Schmuelling,[1] René Rueter,[1] Tabitha Ruecker,[1] Ewelina Betleja,[5] Tao Cheng,[5] Moe R. Mahjoub,[5] Peter Soba,[6,7] Hartmut Schlüter,[4] Eugenio F. Fornasiero,[8] and Froylan Calderon de Anda[1,10,*]

[1]Institute of Developmental Neurophysiology, Center for Molecular Neurobiology, University Medical Center Hamburg-Eppendorf, 20251 Hamburg, Germany
[2]Combinatorial Neuroimaging Core Facility, Leibniz Institute for Neurobiology, 39118 Magdeburg, Germany
[3]Department of Anatomy and Histology, Faculty of Veterinary Medicine, New Valley University, 72511 El-Kharga, Egypt
[4]Institute for Clinical Chemistry and Laboratory Medicine, Mass Spectrometric Proteomics Group, Campus Forschung, University Medical Center Hamburg-Eppendorf, 20246 Hamburg, Germany
[5]Department of Medicine (Nephrology Division), Washington University, St. Louis, MO 63110, USA
[6]LIMES Institute, Department of Molecular Brain Physiology and Behavior, University of Bonn, 53115 Bonn, Germany
[7]Institute of Physiology and Pathophysiology, Friedrich-Alexander-Universität Erlangen-Nürnberg, 91054 Erlangen, Germany
[8]Department of Neuro- and Sensory Physiology, University Medical Center Göttingen, 37073 Göttingen, Germany
[9]These authors contributed equally
[10]Lead contact
*Correspondence: froylan.calderon@zmnh.uni-hamburg.de
https://doi.org/10.1016/j.celrep.2022.110686

SUMMARY

Microtubule (MT) modifications are critical during axon development, with stable MTs populating the axon. How these modifications are spatially coordinated is unclear. Here, via high-resolution microscopy, we show that early developing neurons have fewer somatic acetylated MTs restricted near the centrosome. At later stages, however, acetylated MTs spread out in soma and concentrate in growing axon. Live imaging in early plated neurons of the MT plus-end protein, EB3, show increased displacement and growth rate near the MTOC, suggesting local differences that might support axon selection. Moreover, F-actin disruption in early developing neurons, which show fewer somatic acetylated MTs, does not induce multiple axons, unlike later stages. Overexpression of centrosomal protein 120 (Cep120), which promotes MT acetylation/stabilization, induces multiple axons, while its knockdown downregulates proteins modulating MT dynamics and stability, hampering axon formation. Collectively, we show how centrosome-dependent MT modifications contribute to axon formation.

INTRODUCTION

Neurons are complex cells with distinct functional domains for information processing. In the postsynaptic compartment, dendrites receive synaptic input and relay signals to the soma, where the integrated information is transmitted via the axon over short or long distances. Differentiating neurons follow an intricate process during which one of the neurites is specified as an axon and the remaining become dendrites. Yet the underlying mechanisms of axon selection is incomplete. Pioneering work on the embryonic grasshopper limb showed that the Ti1 neurons extend axons perpendicular to the mitotic cleavage plane (Lefcort and Bentley, 1989). Upon the onset of mitosis in the pioneer mother cell, the MTOC and Golgi tubules are found near the site of the initial axon outgrowth. However, in developing zebrafish embryonic retinal ganglion cells (RGCs), the centrosome position during axon extension is on the opposite to the site of axon formation, at the pole where the future dendrite emerges (Zolessi et al., 2006; Distel et al., 2010). In addition, laminin, as an external cue, helps select the position of axon outgrowth in zebrafish RGCs (Randlett et al., 2011). Along these lines, the secreted UNC-6/netrin protein, which can attract or repel migrating cells and axons, induces neuronal asymmetry in motor neurons of *C. elegans* and defines the site of axon formation (Adler et al., 2006). Nevertheless, an analysis on *Drosophila* sensory neurons suggested that an intrinsic polarization program that relies on the last mitosis from the neuroblast and not only on extracellular cues help define neuronal polarity. A cluster of N-cadherin and furrow markers from the last mitosis of the neuroblast triggers the initial growth of the first neurite (future dendrite), opposite to the centrosome and perpendicular to the last mitotic cleavage plane. Eventually, the centrosome is recruited to the N-cadherin cluster and moves 180° to the tip of the future dendrite. Finally, the axon forms opposite to the N-cadherin/centrosome complex (Pollarolo et al., 2011). In the developing cortex, early electron microscopic studies revealed that the centrosome is generally located at the origin of the extending axon in the multipolar

This is an open access article under the CC BY-NC-ND license (http://creativecommons.org/licenses/by-nc-nd/4.0/).

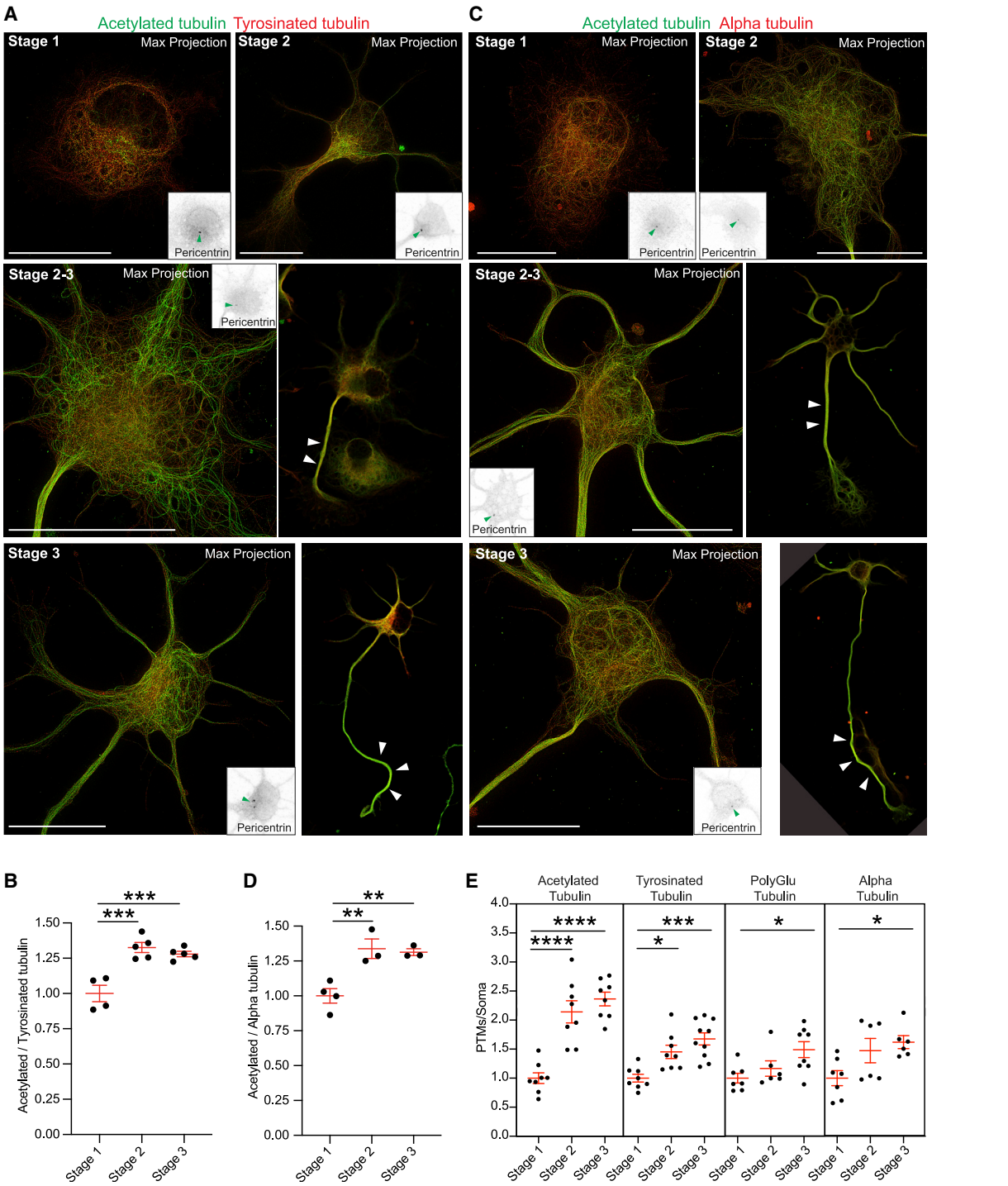

Figure 1. Acetylation of MTs spreads radially from the centrosomal area toward the growing neurites before polarization and significantly into the growing axon after symmetry breakage

(A) STED images of acetylated and TyrTub immunostained hippocampal neurons at stages 1 and 2, transition from stage 2 to stage 3, and stage 3.

(B) STED image quantifications show ratio of acetylated to TyrTub signal area in the soma of stage 1, 2, and 3 neurons.

(C) STED images of acetylated and α-tubulin immunostained stage 1, 2, transition 2–3, and 3 hippocampal neurons.

(D) STED image quantifications show ratio of acetylated to α-tubulin signal area in the soma of stage 1, 2, and 3 neurons.

(E) Area of tubulin PTMs—acetylated, tyrosinated, polyglutamylated tubulin, and α-tubulin—intensities coverage normalized to soma area in stages 1, 2, and 3 neurons.

In (A) and (C), white arrowheads denote AcetyTub enrichment; green arrowhead (insets) denotes centrosome (labeled by pericentrin antibody). Scale bars, 10 μm (A and C). Data in (B), (D), and (E) are represented as mean ± SEM; replicates are distinguished by circles in the graphs. *$p < 0.05$, **$p < 10^{-2}$, ***$p < 10^{-3}$, and ****$p < 10^{-4}$ by one-way ANOVA. See also Figure S1; Videos S1 and S2.

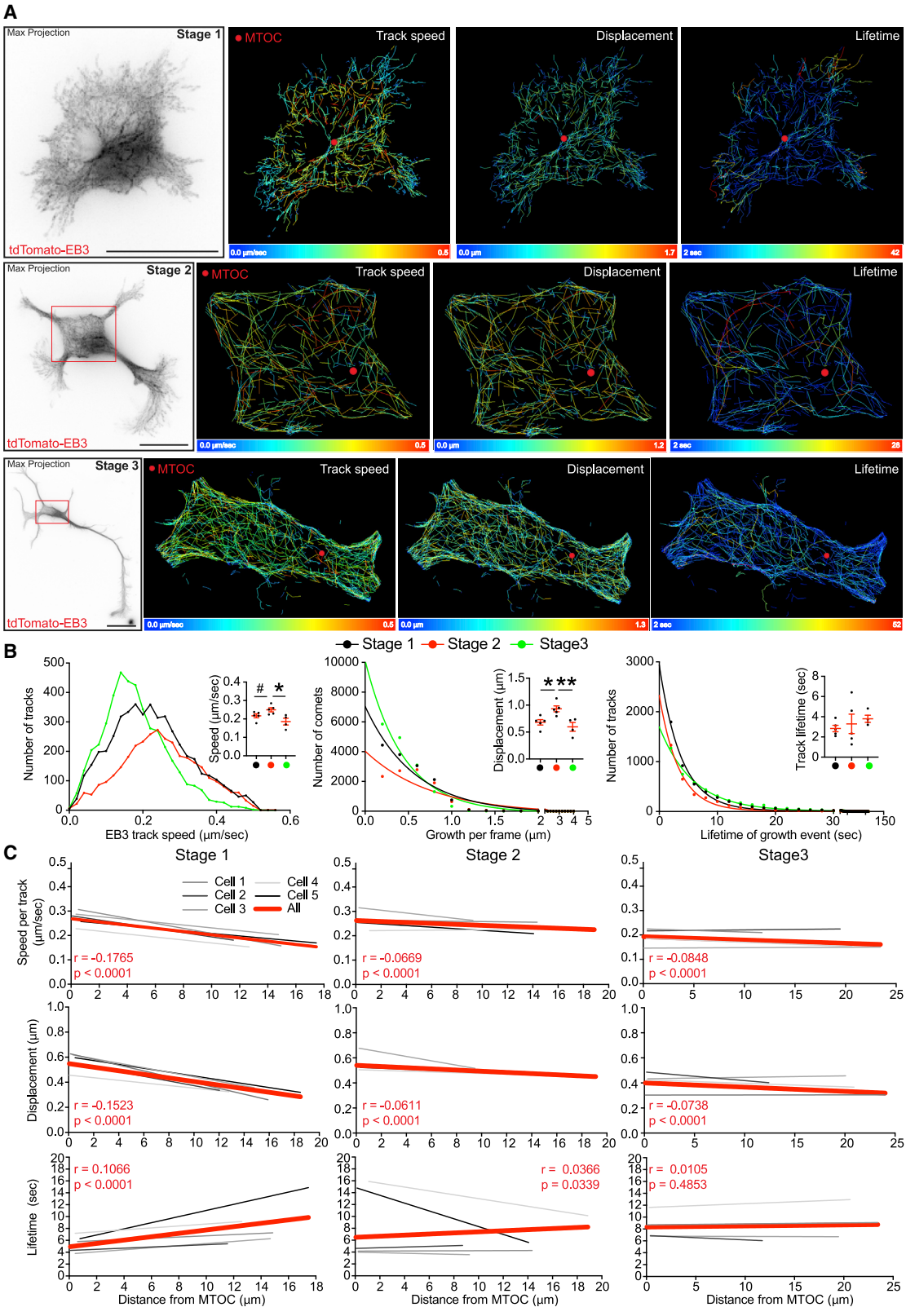

(legend on next page)

neurons of the intermediate zone, which projects tangentially or toward the ventricular zone (Shoukimas and Hinds, 1978). Indeed, live imaging of multipolar cells in the intermediate zone demonstrated that the centrosome translocate transiently to the site of axon formation before or at the time of initial axon outgrowth (de Anda et al., 2010; Sakakibara et al., 2014). Overall, it is possible to envision that axon selection *in situ* is the combination of intrinsic and extrinsic cues. However, the functional role of the centrosome during axon determination has not been extensively tested.

Once the position of axon outgrowth is selected, axon elongation is the defining step for neuronal polarization. Along this line, the neurite with highly dynamic F-actin in the growth cone and more MTs that are eventually stable develops as an axon, whereas the remaining neurites become dendrites (Bradke and Dotti, 1999; Geraldo et al., 2008; Neukirchen and Bradke, 2011; Witte et al., 2008; Yu and Baas, 1994; Zhao et al., 2017; Arregui et al., 1991; Ferreira and Caceres, 1989). In cultured rat hippocampal neurons, the future axon was suggested to have more stable MTs in its shaft (Witte et al., 2008). Accordingly, global application of the MT-stabilizing drug Taxol induced the formation of multiple axons. Moreover, MT stabilization increased F-actin dynamics in growth cones (Zhao et al., 2017). However, the question of how MT stability occurs preferentially in the growing axon remains elusive.

To understand the role of MT stabilization during axon selection, it is crucial to consider if this process is intrinsically mediated or sustained through external cues. Several *in vitro* and *in situ* studies suggest key roles of centrosome-dependent radial MT organization in migrating and early differentiating neurons (Higginbotham and Gleeson, 2007; Kuijpers and Hoogenraad, 2011; Rivas and Hatten, 1995; Schaar and McConnell, 2005; Tsai and Gleeson, 2005; Calderon de Anda et al., 2008; de Anda et al., 2005). Consequently, inhibition of MT nucleation at the centrosome hinders MT reassembly and compromises axonal growth (Ahmad et al., 1994), attributing an important role for the centrosome and its MT assembling ability in axon formation. It is not clear, however, whether the centrosome plays a role for the stabilization/acetylation of MTs in the growing axon. To test this possibility, we performed a series of state-of-the-art experiments including super-resolution imaging, differential quantitative proteomics, and high-content time-lapse microscopy to examine MT organization in early developing neurons.

RESULTS

Radial organization of acetylated MTs in early developing neurons

Axon formation is a hallmark of neuronal polarization in early developing hippocampal and cortical pyramidal neurons (Dotti et al., 1988; de Anda et al., 2010; Namba et al., 2014; Noctor et al., 2004; Sakakibara et al., 2014). Neurons immediately after plating are round forming lamellipodia (stage 1), then they become multipolar extending several neurites (stage 2; Dotti et al., 1988), morphology that is also found in the developing cortex (Noctor et al., 2004; Sakakibara et al., 2014; de Anda et al., 2010; Shoukimas and Hinds, 1978), from which usually the one neurite with the fastest growth rate becomes the axon (stage 3 (Dotti et al., 1988)), while the remaining neurites transform into dendrites (Dotti et al., 1988; Powell et al., 1997). It is known that during the transition from stage 2 to 3, the growth cone of the neurite, which elongates as an axon, contains more dynamic F-actin (Bradke and Dotti, 1999) and more stable MTs (Witte et al., 2008). In accord to previous data of others and our own, we found that in neurons without neurites (stage 1), the position of the centrosome is a landmark to predict the position of axon outgrowth (de Anda et al., 2005, 2010; Zmuda and Rivas, 1998; Andersen and Halloran, 2012). It is not clear, however, if the centrosome contributes with stable MTs in the growing axon at stage 3. To explore this possibility, we decided to perform a detailed analysis of the distribution of acetylated tubulin (AcetyTub) and polyglutamylated tubulin (PolyGluTub), stable MTs versus tyrosinated tubulin (TyrTub) unstable MTs and α-tubulin, to track stable MTs in neurons from stages 1–3. To this end, we used confocal and super-resolution microscopy during early neuronal differentiation *in vitro*. Stimulated emission depletion (STED) microscopy images revealed that stage 1 neurons have the AcetyTub concentrated around the centrosome (labeled with pericentrin), while the polyglutamylated, tyrosinated, or α-tubulin extended over the cell body (Figures 1 and S1; Videos S1 and S2). At stage 2, however, the AcetyTub localizes throughout the cell body, as the polyglutamylated, tyrosinated, or α-tubulin does, and starts to penetrate the neurites (Figures 1 and S1). Neurons that started to extend an axon (stage 3) increased the content of AcetyTub drastically in the longest neurite, presumably the future axon (Figures 1 and S1). These results suggest that a subset of stable/acetylated MTs spreads out radially from the centrosomal area to the growing neurites, eventually concentrating specifically in the longest neurite or future axon.

Figure 2. EB3 dynamics in the soma of developing neurons decrease during polarization: order of magnitude of EB3 dynamics: stage 1 (near MTOC in the soma) > stage 2 cells soma > stage 3 cells soma

(A) Maximum intensity projection images of 5 min time-lapse (1 frame/2 s) of EB3-tdTomato-trasfected stage 1, 2, and 3 hippocampal neurons. EB3 track growth speed, comet displacement (per frame), and track lifetime analyzed using TrackMate/ImageJ plugin. Red dots indicate MTOC.

(B) Left panel: frequency distribution compares speed (μm/s) of EB3 tracks in soma of stage 1, 2, and 3 neurons. Inset: median speed (μm/s). Middle panel: nonlinear fit histogram compares displacement of EB3 (in μm) per each frame (2 s) soma of stage 1, 2, and 3 neurons. Inset: characteristic growth (λ) (half values of displacement) per frame. Right panel: nonlinear fit histogram compares growth lifetime of EB3 tracks (in s) in soma of stage 1, 2, and 3 neurons. Inset: growth half lifetime (τ). Data are represented as mean ± SEM; replicates are distinguished by circles in the bar plots. *$p < 0.05$, **$p < 10^{-2}$, ***$p < 10^{-3}$, and ****$p < 10^{-4}$ by one-way ANOVA. #$p = 0.0654$ by unpaired Student's t test.

(C) Histograms of EB3 track growth speed (μm/s), displacement of EB3 comets (in μm) per each frame (2 s), and growth lifetime of EB3 tracks (in s) in the soma are plotted against the distance from the MTOC, separately, for stages 1, 2, and 3. Black and gray shaded lines, linear regression for individual cells. Red line, mean linear regression for all the cells per stage for which Pearson correlation coefficient (r value) and p value of significance are shown.

Scale bar, 10 μm (A).

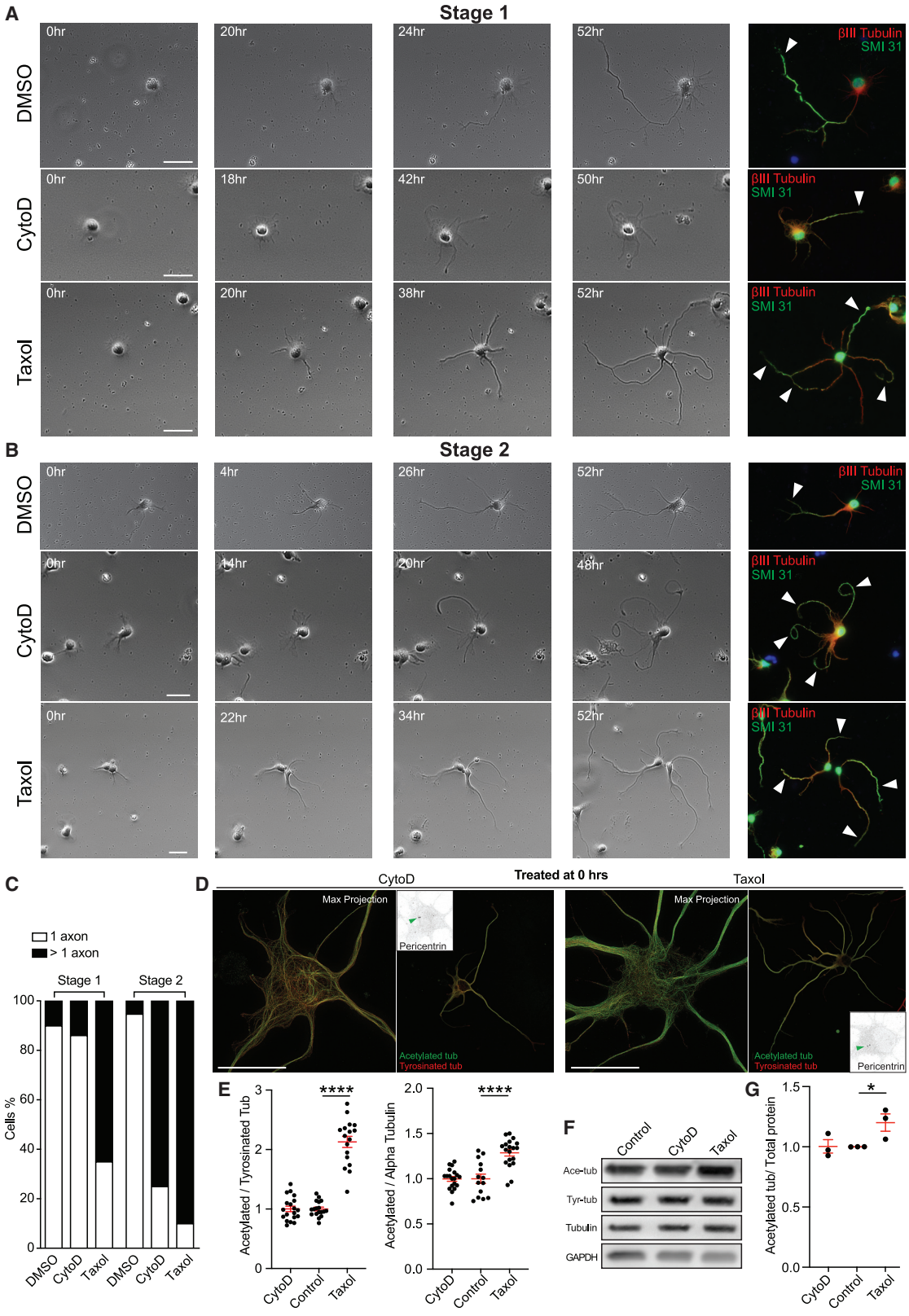

(legend on next page)

Microtube dynamics at the soma differ through the early neuronal development stages

To gain further insight into the relevance of this early somatic MT organization, we decided to monitor growing MTs in the soma of developing neurons. MTs are polarized structures with a plus and a minus end, whereas EB3 is one of three mammalian MT plus-end-binding protein (EB) family members (Komarova et al., 2009). Several parameters related to MT growth can be investigated with live imaging, using EB3 fused to a fluorescent tag (Stepanova et al., 2003). Neurons were transfected with the EB3-tdTomato, and developing neurons (stages 1–3) were imaged. To quantify MT dynamics, we performed semi-automatic tracking of EB3 comets (see STAR Methods) to reconstitute MT tracks and quantified MT track growth speed, displacement of EB3 comet per frame, and track lifetimes (Figure 2A). We plotted the histograms of these parameters and calculated the median of the distribution for the EB3 track speed and fitted the EB3 comet displacement, lifetime with exponential decays (Sironi et al., 2011; Matov et al., 2010; Figure 2B). Our results show that the median growth speed of MTs is increased at stage 2 cells compared with stages 1 and 3 (Figure 2B). The characteristic growth (λ) per frame is higher in stage 2 neurons compared with stages 1 and 3 (Figure 2B). However, the characteristic growth lifetime (τ) did not change across the stages (Figure 2B). These results highlight variable dynamics of somatic MTs during neuronal polarization. Specifically, somatic MTs underwent drastic changes before axon extension, at stage 2.

Close analysis of our cells shows that at stage 1, the somatic MT dynamics vary depending on their distance with the MTOC position. Thus, the speed and length of growing MTs are augmented near the MTOC compared with the soma periphery (Figure 2C). Concerning the growth lifetime of those MTs, we detected a reduced lifetime close to the MTOC (Figure 2C). Once neurons formed neurites, the somatic regional changes regarding MT dynamics were reduced (Figure 2C). Overall, our data show local differences in MT remodeling at the soma of stage 1 neurons. Altogether, our results suggest a radial organization of a subset of stable MTs in the soma that might contribute later to axon formation.

Pharmacological manipulation of the cytoskeleton unmasks the relevance of radial organization of stable MTs

Given our initial observations, we decided to test whether the MT remodeling in the soma influences the extending axon. We therefore hypothesized that if the F-actin cytoskeleton of stage 1 neurons is disrupted, the formation of more than one axon would be precluded because of the lack of stable MTs that could support the extension of multiple axons. F-actin disruption using cytochalasin D (CytoD) is a well-known strategy that challenges neuronal polarity and produces neurons with multiple axons (Bradke and Dotti, 1999). However, it was never tested if the multipolarity induced by CytoD is stage dependent. To this end, we treated hippocampal neurons with 2 μM CytoD right after plating (0 h) and $\sim$30 h after plating for 2 days. At $\sim$30 h after plating, most of the untreated cells were stage 2 neurons (Figures S2B and S2E). Importantly, we found that CytoD treatment of cells at 0 h did not produce multiple axons compared with control DMSO-treated cells (Figures S2A–S2C). However, neurons treated $\sim$30 h after plating increased the proportion of neurons producing multiple axons compared with the DMSO-treated neurons (Figures S2A–S2C). To test if the lack of several axons at 0 h is due to the deficiency of acetylated/stable MTs, we treated cells with the MT-stabilizing drug Taxol at 5 nM concentration for 2 days, which was shown to produce several axons (Witte et al., 2008). According to our hypothesis, Taxol treatment increased the number of cells with multiple axons at both time points 0 and $\sim$30 h compared with control DMSO-treated neurons (Figures S2A–S2C). Furthermore, we left our treated neurons growing for 7 days to further corroborate the axonal identity with AnkG immunostaining (which labels the axon initial segment). We found that cells treated at 0 h with CytoD did not increase the proportion of AnkG-positive processes compared with DMSO-treated neurons (Figures S2D–S2F). Conversely, neurons treated with Taxol at time 0 h produced several AnkG-positive processes (Figures S2D–S2F). These results confirm that the lack of stable MTs at stage 1 is the limiting factor to produce multiple axons in the absence of an organized F-actin cytoskeleton.

Figure 3. Contrary to MT stabilization (by Taxol), F-actin disruption (by CytoD) induced multipolarity is dependent on the developmental stage of the neurons

(A and B) Stage 1 (A) and stage 2 (B) primary rat hippocampal neurons before (0 h) and during 2 μM CytoD or 5 nM Taxol and DMSO treatment for 52 h. Time stamps on phase-contrast images indicate the time elapsed from the start of treatment. Post hoc immunostainings for βIII tubulin and SMI 31 (axonal marker, white arrowheads).

(C) Percentage of stage 1 and stage 2 neurons treated with DMSO or 2 μM CytoD or 5 nM Taxol for 52 h differentiated to have 1 or >1 axon.

(D) STED images of AcetyTub and TyrTub immunostained hippocampal neurons treated with 2 μM CytoD and 5 nM Taxol immediately (0 h) after plating. Insets: centrosome (pericentrin) localization.

(E) Ratio of acetylated to TyrTub (left) and acetylated to α-tubulin (right) signal intensities in the soma of untreated, 2 μM CytoD-treated, and 5 nM Taxol-treated neurons immediately (0 h) after plating and PFA fixed 18 h later.

(F) Western blot images of tubulin PTMs (acetylated, tyrosinated), total tubulin, and GAPDH from rat cortical neuron lysates treated with 2 μM CytoD and 5 nM Taxol immediately (0 h) after plating and cultured for 18 h.

(G) Normalized acetylated to total tubulin levels from rat cortical neuron lysates from untreated, treated with 2 μM CytoD and 5 nM Taxol immediately (0 h) after plating, and cultured for 18 h.

Scale bars, 10 μm (A, B, and D). Data in (E) and (G) are represented as mean $\pm$ SEM; replicates are distinguished by circles in the graphs. *$p < 0.05$ and ****$p < 10^{-4}$ by unpaired t test. See also Figures S2 and S3.

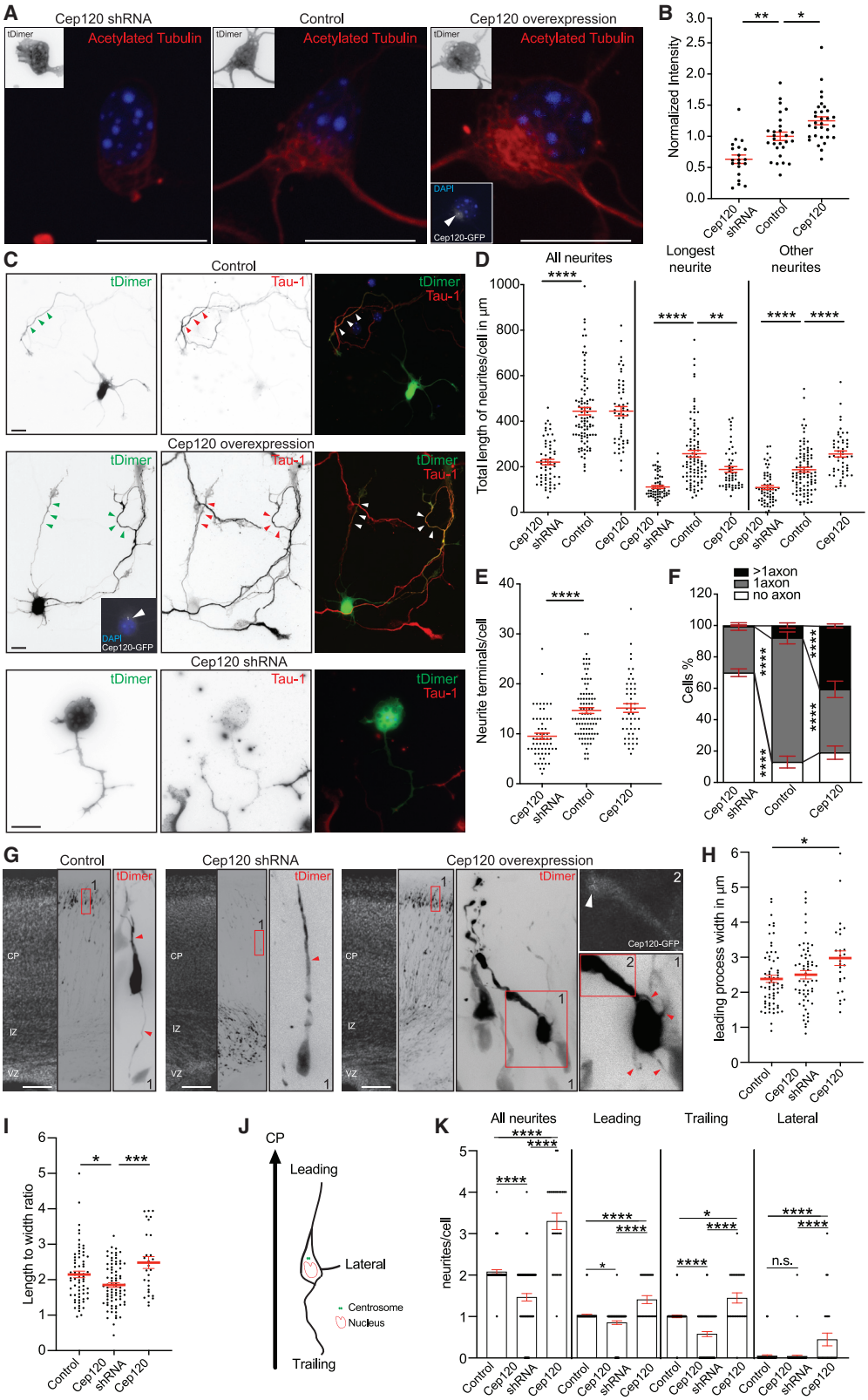

(legend on next page)

Our plated neurons were dissociated from the tissue when they were already differentiating; thus, it is possible that our results could be affected by the redifferentiation process that our cells were subjected to. Therefore, we decided to treat early born neurons and neurons that were already differentiating *in situ*. To this end, we *in utero* electroporated mouse cortices at embryonic day 13 (E13) and at E15 with Venus plasmid and harvested to prepare dissociated cultures at E17. Neurons transfected at E13 were in the cortical plate of the developing cortex; hence, they were migrating and quite advanced in their differentiation process (Figure S2G). Conversely, when cortices were transfected at E15, early born neurons were in the lower intermediate zone initiating their differentiating program (Figure S2G). Independently of the *in situ* developmental stages, we found that cortical cells treated with CytoD at time 0 h do not form multiple axons, as we documented with the hippocampal neurons (Figure S2H). When cultured neurons were treated with Taxol, however, they increased the proportion of multiple axons (Figure S2H).

Furthermore, we performed a long-term time-lapse analysis of stage 1 and 2 hippocampal neurons treated with CytoD and Taxol. We corroborated that the stage 2 neurons, but not stage 1 cells, treated with CytoD produce multiple axons, as the Taxol treatment does (Figures 3A–3C). Finally, we verified that cells treated with CytoD at 0 h, right after plating, have fewer somatic acetylated MTs (STED images and confocal microscopy analysis; Figures 3D and 3E) as well as total AcetyTub (western blot [WB] analysis; Figures 3F, 3G, and S3A) compared with cells treated with Taxol. When cells were treated ~30 h after plating, however, CytoD induced a significant increment in AcetyTub compared with control cells (Figures S3B and S3C). Regarding PolyGluTub, we could not detect an increment of this MT modification by WB analysis after Taxol treatment at 0 h (Figures S3D and S3E). However, PolyGluTub increased in the soma, when normalized with TyrTub, upon Taxol treatment at 0 h (Figure S3F). Interestingly, the PolyGluTub/α-tubulin ratio in the soma decreased after Taxol treatment at 0 h in contrast to the acetyl/α-tubulin levels (Figure S3F). Overall, our results suggest that somatic acetylated MTs enrichment drives axon formation.

Centriolar protein Cep120 modulates MTs stability and axon formation

To understand mechanistically how the centrosome regulates MTs dynamics and axon formation, we decided to interfere with the expression of Cep120, a centriolar protein, which was shown to affect MT stability (de Anda et al., 2010; Xie et al., 2007; Joseph et al., 2018; Betleja et al., 2018). Cep120 has been previously shown to control the size of the astral MT structure, which couples the centrosome and the nucleus in neuronal progenitors (Xie et al., 2007). In addition, it has been shown that Cep120 controls MT stability in developing neurons (de Anda et al., 2010). Moreover, Cep120 modulates cilia formation and lack of Cep120 impairs centriole maturation, cilia elongation, and MT acetylation on the cilia (Joseph et al., 2018; Betleja et al., 2018). Cep120 is therefore a suitable molecule to evaluate whether the centrosome-dependent organization of MTs supports axon formation. We analyzed the presence of Cep120 in developing neurons in culture and found that it is present throughout stages 1–3 (Figures S4A and S4B). Moreover, it localizes adjacent to the cilia, immunolabelled by Arl13b (Figure S4C). To investigate the effects of Cep120 downregulation in early neuronal development, we used Cep120 shRNA construct for specifically silencing Cep120 expression in cortical neurons (Figures S4D and S4E; de Anda et al., 2010). To this end, we introduced Cep120 short hairpin RNA (shRNA) or control shRNA plasmids together with tDimer expressing plasmid in mice brain cortices at embryonic day 15 and isolated cortical neurons at E17. In parallel, Cep120 was over-expressed using Cep120-GFP together with tDimer expressing plasmid (Figures S4D and S4E). Neurons were cultured for an additional 48–72 h, fixed, and prepared for immunostaining to assess MT modifications and cell morphology. Our results show that Cep120 downregulation decreased the levels of AcetyTub (Figures 4A and 4B), PolyGluTub, TyrTub, and total tubulin (Figure S5A) content in the soma compared with the control-transfected neurons. On the contrary, Cep120 overexpression significantly increased the levels of AcetyTub (Figures 4A and 4B), but not of PolyGluTub, TyrTub, and total tubulin (Figure S5A), in the soma compared with the controls. These results suggest that Cep120 overexpression regulates the formation of a

Figure 4. Cep120 knockdown and overexpression, through MT acetylation, bidirectionally regulates axon formation

(A) Confocal maximum projection images of mouse cortical neurons co-transfected at E15 via IUE with tDimer and Cep120 shRNA, or control or Cep120-GFP (arrowhead in the inset) cultured at E17 for 48 h immunostained with AcetyTub antibody.

(B) Normalized AcetyTub intensities in the soma of neurons expressing Cep120 shRNA, control, and Cep120-GFP as shown in (A).

(C) Epifluorescence images of mouse cortical neurons co-transfected via IUE at E15 with tDimer and Cep120 shRNA or control or Cep120-GFP (indicated by arrowhead in the inset) cultured at E17 for 48 or 72 h immunostained with Tau-1 antibody to confirm the axonal identity of the neurites, indicated by white arrowheads.

(D and E) Quantification of neurite length (in μm) (D) and neurite terminals (E) expressing Cep120 shRNA, control, and Cep120-GFP as shown in (C).

(F) Percentage of Cep120 shRNA, control, and Cep120-GFP neurons, as shown in (C), differentiated to have no axon, 1 axon, and >1 axon. Data shown in (B), (D), (E), and (F) are obtained from cortical cultures of 3 or more IUE embryos from at least 2 different mothers.

(G) E19 mouse cortical slices co-transfected via IUE at E15 with tDimer and Cep120 shRNA or control or Cep120-GFP. Red insets (labeled 1): zoomed view of migrating neurons in the cortical plate from respective groups. Red arrowheads in insets 1: apical, basal, and lateral neurites. White arrowheads in inset 2: Cep120-GFP signal.

(H) Leading process width (in μm) of neurons in the cortical plate expressing Cep120 shRNA, control, and Cep120-GFP.

(I) Length-to-width ratio of the soma of neurons in the cortical plate expressing Cep120 shRNA, control, and Cep120-GFP expressing neurons.

(J) Schematic illustration of apical, basal, and lateral neurites of a migrating neuron used for analyzing data in (K).

(K) Neurite number quantifications of neurons in the cortical plate expressing Cep120 shRNA, control and Cep120-GFP expressing neurons.

Data shown in (H), (I), and (K) are obtained from three E19 mouse brains slices from two Cep120-GFP and three control and three Cep120 shRNA embryonic mouse brains. Scale bars, 10 μm (A and C) and 200 μm (G). Data in (B), (D), (E), (F), (H), (I), and (K) are represented as mean ± SEM; replicates are distinguished by circles in the graphs, except in (F). *$p < 0.05$, **$p < 10^{-2}$, and ****$p < 10^{-4}$ by one-way ANOVA. See also Figures S4 and S5.

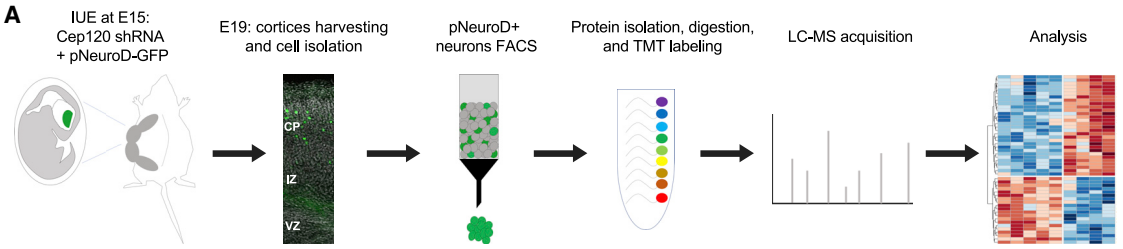

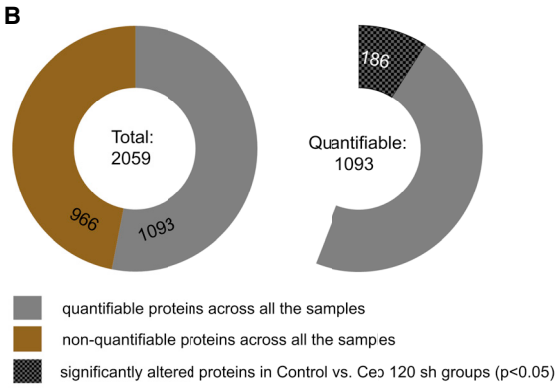

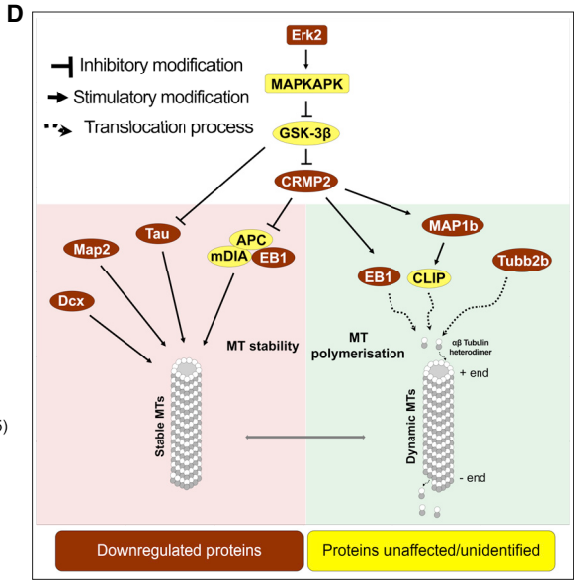

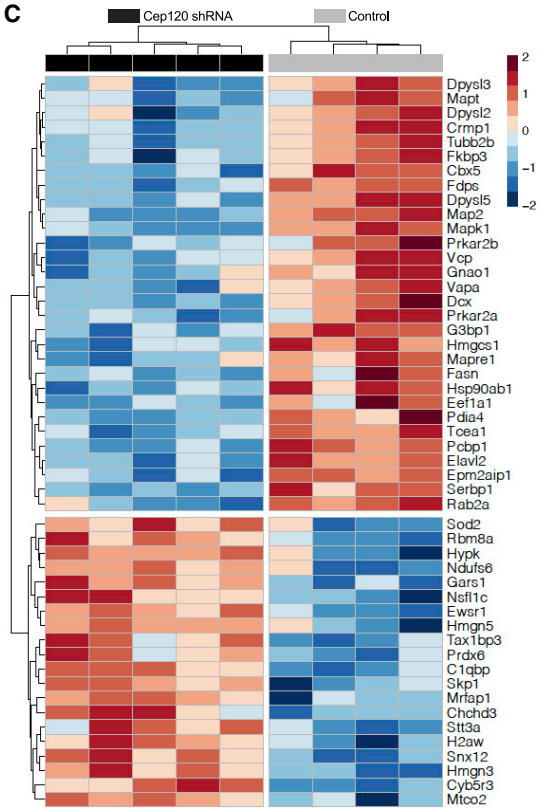

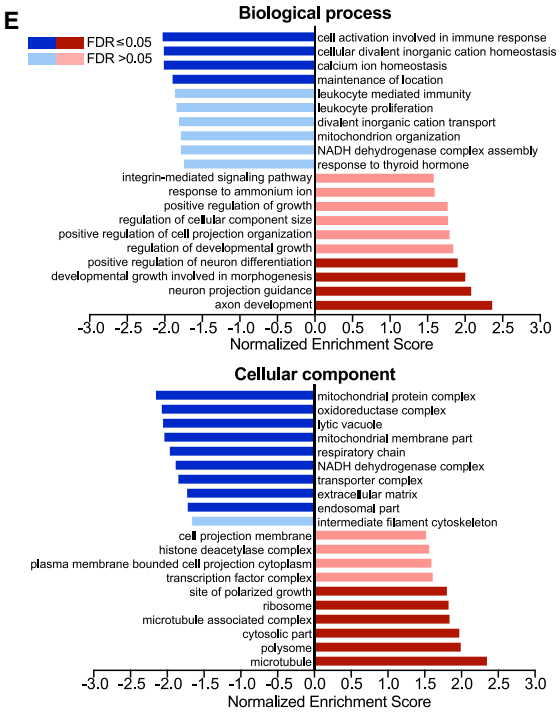

(legend on next page)

subset of stable (acetylated) MTs. To test this, we treated cells expressing Cep120 shRNA or Cep120-GFP with a short pulse of nocodazole, which affects MT polymerization. Our results show that Cep120 overexpression protected MTs against the depolymerization effect of nocodazole (Figures S5B and S5C). Importantly, we found that Cep120 overexpression produced neurons with more than one axon and, overall, more complex neurons with increased length of neurites per cell, compared with control neurons (Figures 4C–4F). Conversely, Cep120 downregulation precluded axon formation and decreased the complexity of the neurons withfewer neurites per cell, and reduced neurite length (Figures 4C–4F). Finally, we asked whether Cep120 is necessary and sufficient for axon formation. To assess this, we treated neurons lacking Cep120 with Taxol to test whether MT stabilization is enough to overcome the lack of this centriolar protein. Indeed, the Taxol treatment was unable to overcome the lack of Cep120, and those cells failed to form multiple axons as the Taxol-treated control cells did (Figure S5D). Taken together these experiments point out an important role of Cep120 in axon formation and MTs acetylation as previously shown for the cilia formation (Joseph et al., 2018; Betleja et al., 2018).

To further investigate the role of Cep120 on neuronal differentiation *in vivo*, we decided to overexpress or downregulate Cep120 in the developing cortex. In previous work, we found that specific downregulation of Cep120 in the developing cortex precludes axon formation and impairs neuronal migration (de Anda et al., 2010). It was not investigated, however, whether the Cep120 overexpression affects neuronal development *in vivo*. To test this, we *in utero* electroporated cortices with Cep120 shRNA or Cep120 overexpressing plasmids together with tDimer plasmid at E15, and brains were harvested at E19. We specifically analyzed the migrating neurons in the cortical plate (CP) when they already should have formed an axon (Figures 4G–4K). Our results show that Cep120 downregulation leads to alterations of the cell body morphology with a reduction of the length to width ratio compared with control-transfected neurons (Figures 4G–4I). In addition, we detected a diminution of bipolar neurons at the CP without trailing process or future axon compared with control neurons (Figures 4G, 4J, and 4K). In a few neurons, we also observed that Cep120 downregulation precluded the formation of a leading process (Figure 4K). On the contrary, Cep120 overexpression produced migrating neurons in the CP with increased width of the leading process (Figures 4G and 4H). Some Cep120-transfected neurons bear more than one leading process or trailing process, and overall, the neurons overexpressing Cep120 have processes emerging laterally from the cell body, the lateral processes, that the control and Cep120 shRNA transfected neurons rarely have (Figures 4G, 4J, and 4K). Altogether these results demonstrate that Cep120 downregulation or overexpression has a bidirectional effect on the morphological complexity of migrating neurons in the CP.

Lack of Cep120 affects the landscape of proteins regulating MT dynamics

To test more directly the effect of Cep120 downregulation, we decided to measure the proteome in the absence of Cep120 *in vivo*. To this end, we *in utero* electroporated cortices at E15 with Cep120 shRNA or control along with pNeuroD-GFP (which is expressed exclusively in neurons; de Anda et al., 2010), at E19 brains were harvested, and GFP-positive cells were FAC-sorted. Afterward, cells were prepared for differential quantitative proteomics and bioinformatics analyses (Figure 5A). Our results show that from the 1,093 quantifiable proteins, 186 were significantly altered after Cep120 downregulation (Figure 5B). Interestingly, among these several proteins associated with MT dynamics were downregulated in the absence of Cep120, such as Map2, Tau, EB1, Dcx, CRMP2, MAP1b, and Tubb2b, among others (Arimura and Kaibuchi, 2007; Conde and Caceres, 2009; Figures 5C, 5D, and S6A). Finally, Gene Ontology (GO) analysis supported this general impression, as several categories linked to axonal elongation and formation were enriched in the control sample versus neurons missing Cep120. In detail, gene set enrichment analysis (GSEA) across all identified proteins across the two samples indicates that categories such as axon development (biological process), site of polarized growth, MT associated complex, and MT (cellular component) were significantly enriched in control samples versus neurons missing Cep120 (Figure 5E). Altogether, these results suggest substantial changes to the proteome landscape of neurons without Cep120, which might affect MTs dynamics and axon formation/extension.

Manipulation of Cep120 levels affects MT dynamics

To test if Cep120 manipulation affects MT dynamics, we decided to monitor growing MTs by time-lapse microscopy using EB3-tdTomato. Cortices were *in utero* electroporated at E15 with Cep120 shRNA + EB3-tdTomato or Cep120-GFP + EB3-tdTomato, and cells were plated at E17. Our results show that the median growth speed of MTs is increased significantly after Cep120 overexpression compared with control-transfected

Figure 5. Cep120 knockdown downregulates key proteins related to MT stability and dynamics, revealed by differential quantitative mass spectrometric proteome analysis of migrating cortical neurons

(A) Scheme of different steps in the proteome analysis on migrating cortical neurons at E19 transfected via IUE at E15 with control or Cep120 shRNA along with pNeuroD-GFP plasmid.

(B) Illustration of 2,059 proteins identified in the proteome analysis across all the samples: n = 4 for controls and n = 5 for Cep120 shRNA condition, of which 1,093 are quantifiable and 186 are significantly ($p < 0.05$) altered proteins.

(C) Heatmap of 50 significantly altered proteins in the samples from control versus Cep120 knockdown conditions with the lowest significant p value (<0.05).

(D) Pathway illustrates key proteins that are downregulated upon Cep120 knockdown, obtained from the top 50 altered proteins list with the lowest significant p value (<0.05) shown in (C). Alternative names of proteins listed in the pathway: Erk2 = MAPK1, CRMP2 = Dpysl2, Tau = MAPT, and EB1 = Mapre1.

(E) GSEA of control samples versus Cep120 shRNA resuming the results the two non-redundant functional ontology databases: biological process and cellular component. FDR, false discover rate.

See also Figures S6, S7A, and S7B; Tables S1, S2, and S3.

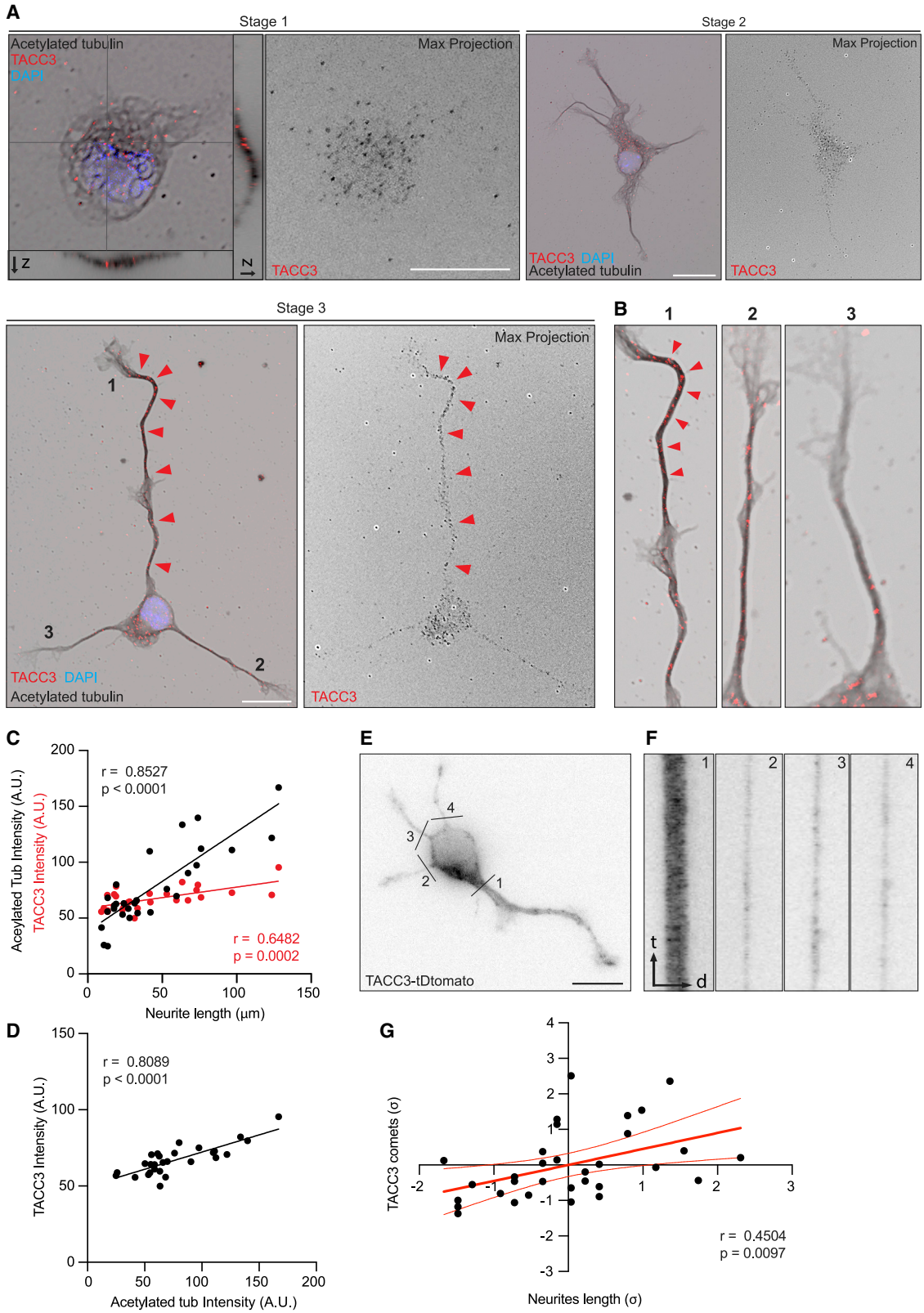

(legend on next page)

neurons (Figures S7A and S7B). Likewise, the characteristic growth per frame (λ) shows higher EB3 comet displacement when Cep120 is over-expressed (Figures S7A and S7B). Finally, we analyzed the characteristic lifetime (τ) per cell, and no significant differences were detected between the groups (Figures S7A and S7B). These results highlight that overexpression of Cep120 levels lead to increased MT dynamics.

Previously, it was shown that Cep120 in coordination with the transforming acid coiled-coil protein 3 (TACC3), which is a MT plus-end protein (Nwagbara et al., 2014), promotes the elongation of the MT aster in neuronal progenitors (Xie et al., 2007). TACC3 functions at the centrosome regulating MT nucleation, along the MT lattice to stabilize the spindle apparatus, and at the MT plus-end to promote mitotic spindle elongation (Gergely et al., 2000; Kinoshita et al., 2005; Mortuza et al., 2014). Moreover, TACC3 promotes axon elongation and regulates MT plus-end dynamics and stability (Furey et al., 2020; Erdogan et al., 2017; Nwagbara et al., 2014). Here we show, in cultured neurons, that endogenous TACC3 is present in the neurite shaft following a positive correlation with neurite length and with AcetyTub (Figures 6A–6D); thus, TACC3 is enriched in the longest neurite (future axon) of stage 3 neurons. Furthermore, time-lapse analysis shows that TACC3 comets move anterogradely in a graded manner, with the longest neurites receiving more (Figures 6E–6G). These observations suggest a differential radial MTs stability that may depend on the presence of TACC3.

Cep120 overexpression partially restores MTs acetylation and promotes axon formation in TACC3-inhibited cells

We decided to test whether Cep120 could restore MT dynamics, and thus axon formation, when TACC3's function is inhibited. In order to test this, we used a TACC3 inhibitor (SPL-B) that is previously known to selectively inhibit the nucleation of centrosome MTs (Yao et al., 2014). We found that SPL-B decreased the somatic content of acetylated MTs compared with control-treated neurons (Figures 7A and 7B). However, overexpression of Cep120 partially rescued the content of somatic acetylated MTs in the presence of SPL-B (Figures 7A and 7B). Interestingly, the somatic PolyGluTub content that is reduced in the presence of SPL-B has not been rescued by the overexpression of Cep120 (Figure 7B). These results further support the role of Cep120 modulating only a subset of stable MTs (i.e., acetylated MTs).

Finally, we observed that SPL-B treatment decreased the length and number of neurites per cell and precluded axon formation (Figures 7C–7F). Similar results were obtained when TACC3 was downregulated with already published and validated shRNA sequence (Furey et al., 2020; Figures S7C–S7F). Importantly, Cep120 overexpression partially overcomes these SPL-B-dependent deficits, and neurons initiated to form neurites and to extend an axon (Figures 7C–7F). Altogether, these results demonstrate a synergistic function of Cep120 and TACC3 and insufficiencies of either of these proteins preclude neuronal differentiation and axon formation.

DISCUSSION

MT post-translational modifications (PTMs), specifically acetylation, polyglutamylation, and other PTMs, have crucial roles in the assembly, maintenance, and function of complex and stable MT-based organelles that form the core components of the centrosome such as the centrioles, basal bodies (the protein structure at the base of a cilium or flagellum), and axonemes (the central strand of a cilium or flagellum) (reviewed in Wloga et al., 2017). In addition, various studies point out the presence of stable MTs in axons, determined by measuring acetylated (Witte et al., 2008) or deTyrTub (Arregui et al., 1991).

Selective translocation of the Kinesin-1 motor domain into the nascent axon was described as one of the earliest events during axon elongation (Jacobson et al., 2006). Tubulin acetylation and detyrosination were shown to be required for Kinesin-1 motor domain translocation into the axons (Konishi and Setou, 2009; Reed et al., 2006). A later study, however, showed that acetylation of MTs itself is not enough for sorting of Kinesin-1 into axons (Hammond et al., 2010). Moreover, Taxol-induced translocation of Kinesin-1 into supernumerary axons correlated with the enhancement of three different MT PTMs (acetylation, detyrosination, and glutamylation; Hammond et al., 2010). Overall, it seems that axons contain a higher percentage of stable MTs compared with their dendritic counterparts (reviewed in Baas et al., 2016). Yet the exact mechanisms by which differential MT stability is achieved in axons versus the other minor neurites that will eventually become dendrites are not clear.

Our results demonstrate that before axon extension, the soma contains acetylated MTs preferentially surrounding the centrosome. Once neurites are formed, the acetylated MTs penetrate

Figure 6. TACC3 is enriched in the longer neurites in developing neurons during neuronal polarization

(A and B) Maximum projection images showing TACC3 localization in developing rat hippocampal neurons, stage 1, 2, and 3 neurons, co-stained with AcetyTub shown in (A). Red arrowheads, TACC3 enrichment in the longest neurite of a stage 3 cell. Zoom images of neurites 1, 2, and 3 labeled in stage 3 cell are shown in (B).

(C and D) Correlation of TACC3 and AcetyTub intensities in the neurites of developing rat hippocampal neurons. (C) Linear regression analysis of TACC3 and AcetyTub intensities in neurites versus length of the corresponding neurites in stage 2 (or 3) neurons. (D) Linear regression of TACC3 versus AcetyTub intensity values obtained from the same neurites of stage 2 (or 3) neurons. Pearson correlation coefficient (r value) and p value of significance are as indicated in the respective graphs.

(E and F) Maximum intensity projection (black-on-white images) from a 5 min time-lapse (1 frame every 2 s) of a developing rat hippocampal neuron nucleofected with tdTomato-TACC3 in (E). Kymographs obtained from neurite shafts shown in (F); location indicated by black lines 1–4 in (E).

(G) Linear regression analysis of neurite length and TACC3 comets number entering the neurites (per 5 min) from stage 2 and early stage 3 cells; values were normalized according to standard score, and axes are represented in units of SD (σ). Pearson correlation coefficient (r value) and p value of significance are as indicated. Thin red lines denote 95% confidence intervals.

Scale bar, 10 μm (A and E).

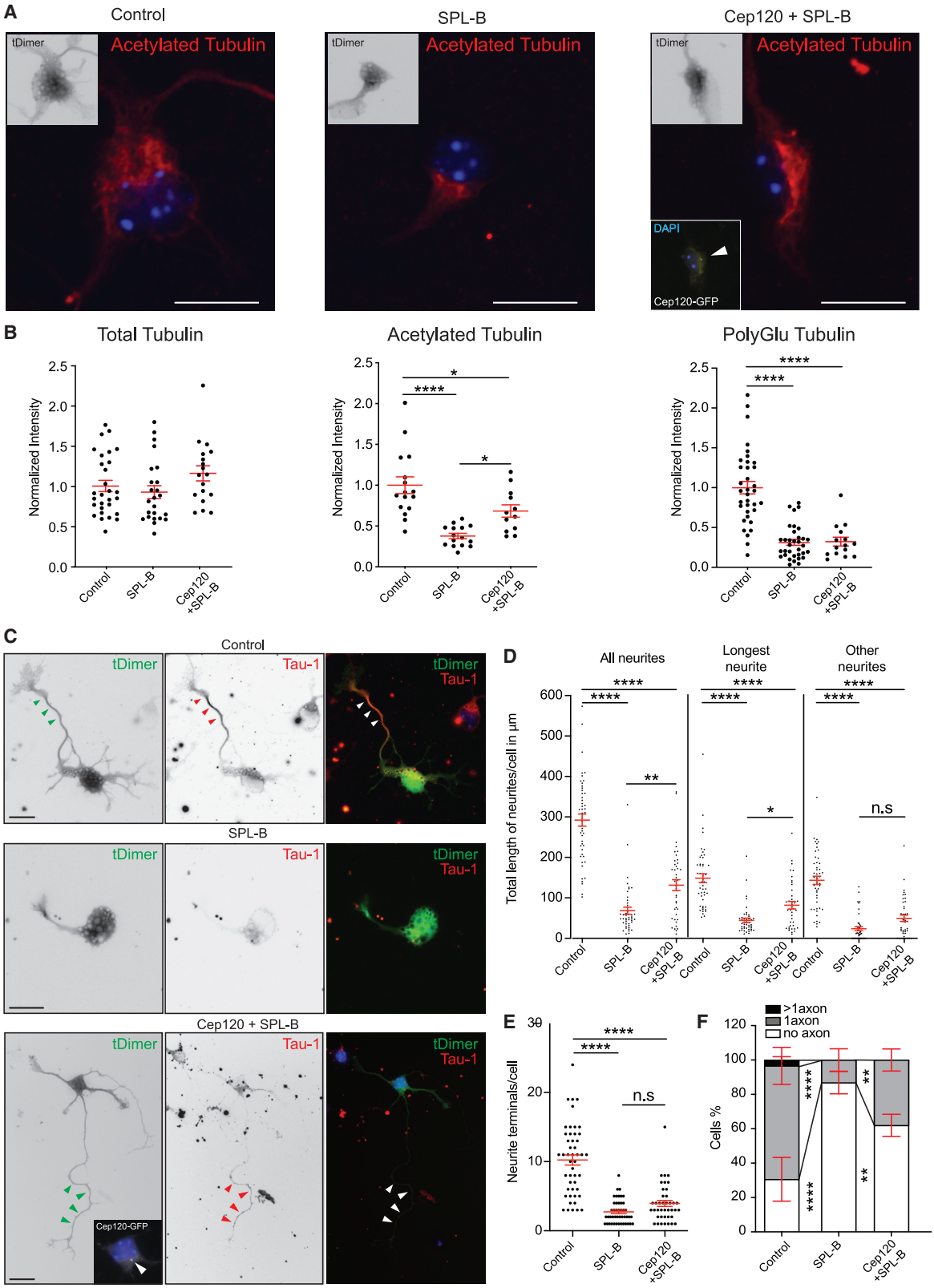

(legend on next page)

them and eventually enriched in the growing axon. This initial somatic MT organization might set the conditions to break the symmetry once the axonal fate is defined. Importantly, PolyGluTub, unlike AcetyTub, does not follow an initial radial organization; thus, at stage 1 this PolyGluTub is rather spread out more in the cell body, not concentrated around the centrosome. These observations suggest involvement of specific tubulin PTMs in the establishment of early axonal identity.

Supporting the initial graded distribution of AcetyTub, we uncovered differential effects of CytoD, a drug that is known to induce multiple axons by causing F-actin disruption, on stage 1 and stage 2 cells. Unlike Taxol, that promotes MT stability, CytoD does not induce multiple axons in the less developed stage 1 cells, with relatively fewer stable MTs in the soma. Moreover, we found that Cep120, a centriolar protein that promotes MTs stability (Joseph et al., 2018; Betleja et al., 2018; Tsai et al., 2019), affects axon formation. Importantly, we could show that the levels of Cep120 modulate axon formation in a bidirectional manner. On one hand, lack of Cep120 precluded axon formation; on the other hand, excess of Cep120 produced neurons with multiple axons. Importantly, cells lacking Cep120, although treated with the MT-stabilizing drug Taxol, fail to form multiple axons, thus supporting the view of a radial organization of AcetyTub. Accordingly, Cep120 overexpression increased somatic levels of AcetyTub, but not PolyGluTub, and protected them from the depolymerization effect of nocodazole. Furthermore, we found that the plus-end protein TACC3, which binds Cep120 (Xie et al., 2007) and affects MT stability (Furey et al., 2020; Erdogan et al., 2017; Nwagbara et al., 2014), is present in the neurite shaft. TACC3 also shows a positive correlation with neurite length and with AcetyTub; thus, it is enriched in the longest neurite (i.e., future axon) of stage 3 neurons. Along these lines, time-lapse analysis shows TACC3 comets move anterogradely in a graded manner with the longest neurites receiving more, suggesting differential radial MTs stability. Finally, Cep120 overexpression partially rescued the effect of SPL-B, a TACC3 inhibitor that selectively inhibits the nucleation of centrosome MTs, only on the AcetyTub but not the PolyGluTub. Altogether, our results suggest that centrosomal functions/Cep120 in synergy with TACC3 might contribute to MTs acetylation in a centrifugal manner.

MT dynamics versus PTMs

We found in early differentiating neurons (stage 1) regional somatic MT dynamics with increased growth speed and length near the MTOC and decreased lifetime of the EB3 trajectories. This suggests highly dynamic MTs near the MTOC. In fixed samples, we detected preferentially acetylated MTs near the centrosome, which would in contrast indicate more stable MTs in this region. Of note, how tubulin acetylation interferes with MT polymerization dynamics is a long-standing question. In this regard, it was shown that promoting tubulin acetylation pharmacologically did not alter MT dynamics (e.g., growth rate and shortening rate) (Matov et al., 2010). Nevertheless, the acetylated MTs were more resistant to the depolymerization effects of nocodazole (Matov et al., 2010). Consequently, stable MTs do not forcefully imply fewer dynamic MTs, and our observations are only in apparent disagreement.

At later stages, we could not uncover somatic regional differences regarding speed, length, or lifetime of growing MTs. However, at stage 2, before axon formation, we detected an overall increment of somatic EB3 speed and track length. Similarly, stage 2 cells overexpressing Cep120, which eventually formed multiple axons, showed an increment in those parameters compared with control cells. Overall, these results suggest local MT remodeling at stage 1, whereas at stage 2 more drastic changes would take place in the soma to set the conditions for symmetry breakage, leading to axon elongation.

Centrosome functions during axon elongation

Once the axon is growing, the organization of MT arrays shifts from centrosome dependent to centrosome independent in hippocampal neurons in culture, as also confirmed by the fact that centrosome ablation during axon elongation does not affect axon extension or regeneration (Stiess et al., 2010). Yet centrosome ablation in stage 2 and early stage 3 neurons decreased the content of somatic growing MTs (Meka et al., 2019). Furthermore, centrosome ablation in neurons developing *in vivo*, before any sign of axon development, preclude axon formation (Andersen and Halloran, 2012). In more developed stage 3 neurons, however, there is decentralization of centrosomal proteins, such as γ-tubulin, which in turn can organize acentrosomal MTs in older neurons (Stiess et al., 2010). Along these lines, Augmin and γ-TuRC are shown to be crucial for uniform plus-end out MT polarity in axons of matured neurons (Sanchez-Huertas et al., 2016). Even though it is still not clear how MT remodeling shift from a ''centrosomal'' to an ''acentrosomal'' manner, our data clarify how early centrosome-dependent MT acetylation contributes to axon formation.

Limitations of the study

In this report we do not address the pathways by which Cep120 downregulation affected the levels of MT stability-related proteins (e.g., Tau, CRMP2). It is plausible to envision either a

Figure 7. Cep120 overexpression partially rescues SPL-B-induced axon loss phenotype by promoting MT acetylation

(A) Maximum projection images of mouse cortical neurons co-transfected via IUE at E15 with tDimer alone or together Cep120-GFP (indicated by arrowhead in the inset) cultured at E17 were treated immediately after plating with 0.25 μg/mL SPL-B, a TACC3 inhibitor, for 48 h immunostained with AcetyTub antibody.

(B) Normalized total tubulin, AcetyTub, and polyglutamylated tubulin intensities in the soma of control, SPL-B-treated, and SPL-B-treated Cep120-GFP neurons.

(C) Epifluorescence images of mouse cortical neurons co-transfected via IUE at E15 with tDimer alone or together Cep120-GFP (arrowhead in the inset) cultured at E17 were treated immediately after plating with 0.25 μg/mL SPL-B for 48 h immunostained with Tau-1 antibody, indicated by white arrowheads.

(D and E) Quantification of neurite length (in μm) (D) and neurite terminals (E) of control, SPL-B-treated, and SPL-B-treated Cep120-GFP neurons.

(F) Percentage of control, SPL-B-treated, and SPL-B treated Cep120-GFP neurons differentiated to have no axon, 1 axon, or >1 axon.

Data shown in (B), (D), (E), and (F) are obtained from cortical cultures of 3 or more IUE embryos from at least 2 different mothers. Scale bars, 10 μm (A and C). Data in (B), (D), (E), and (F) are represented as mean ± SEM; replicates are distinguished by circles in the graphs, except in (F). *$p < 0.05$, **$p < 10^{-2}$, and ****$p < 10^{-4}$ by one-way ANOVA. See also Figures S7C–S7F.

parallel pathway or further downstream signaling modulating MT modifications indirectly. The exact molecular mechanisms by which Cep120 orchestrates the levels of these proteins remain for the moment undetermined.

Importantly, our data do not describe the exact mechanisms by which MT acetylation radially spreads into the growing axon. It is possible that the stable pool of MT is transported from the cell body into growing axons following a sliding filament model, as previously shown (Guha et al., 2021; He et al., 2005; Rao et al., 2017; Slaughter et al., 1997). Alternately TACC3 or other proteins might contribute to MT acetylation/stability distally, far from the centrosome, by promoting the formation of long-live MTs (Nwagbara et al., 2014; Furey et al., 2020).

STAR★METHODS

Detailed methods are provided in the online version of this paper and include the following:

SUPPLEMENTAL INFORMATION

Supplemental information can be found online at https://doi.org/10.1016/j.celrep.2022.110686.

ACKNOWLEDGMENTS

We thank M. Richter (Calderon lab, Zentrum für Molekulare Neurobiologie Hamburg [ZMNH], Universitätsklinikum Hamburg-Eppendorf [UKE]), I. Hermans-Borgmeyer (ZMNH, UKE), and the members of animal facility at the UKE Hamburg for their help with animal experiments. Thanks to the members of Cytometry & Cell Sorting Core Unit, Stem Cell Transplant Clinic, Oncology Center at the UKE for fluorescence-activated cell sorting (FACS) experiments. F.C.A. is supported by Deutsche Forschungsgemeinschaft (DFG) grants FOR 2419, CA1495/1-1, CA 1495/4-1, and CA 1495/7-1; ERA-NET Neuron Grants (Bundesministerium für Bildung und Forschung [BMBF] 01EW1410, 01EW1910, and 01 EW2108B), a JPND Grant (Bundesministerium für Bildung und Forschung 01ED1806), and the University Medical Center Hamburg-Eppendorf (UKE). D.P.M. is a co-applicant in the DFG Grant CA 1495/4-1 for F.C.A. M.H. is partially funded by a scholarship (ID: seventh plan 2012–2017) from the Cultural Affairs and Missions Sector, Ministry of Higher Education of the Arab Republic of Egypt. P.S. is supported by the DFG Heisenberg programm (SO 1337/6-1), DFG (SO 1337/2-2, SO 1337/4-1, SO 1337/7-1), and ERA-NET Neuron (Bundesministerium für Bildung und Forschung 01EW1410 and 01EW1910). E.F.F. is supported by a Schram Stiftung (T0287/35359/2020) and a DFG grant (FO 1342/1-3).

AUTHOR CONTRIBUTIONS

F.C.A. conceived the idea and supervised the project. F.C.A. and D.P.M. designed research and interpreted the data. B.S. conducted cell culture work. O.K. and D.P.M. performed STED microscopy. O.K. did the deconvolution. F.C.A. and D.P.M. performed the analysis. D.P.M. and F.C.A. performed *in utero* electroporation (IUE) surgeries. D.P.M., S.H., C.M.F., N.S., S.W., B.S., and R.R. performed all immunostainings. D.P.M. and N.S. did all epifluorescence imaging. D.P.M., S.H., C.M.F., S.W., N.S., and F.C.A. did the analysis. D.P.M. performed EB3/TACC3 comet live imaging and analysis. D.P.M. did spinning disk imaging and analysis of primary neurons and *in situ* experiments. E.F.F. performed the long-term time-lapse acquisitions, post hoc SMI 31 immunostainings, and imaging. D.P.M. quantified the data. M.H. performed western blots. E.B., T.C., and M.R.M. developed the Cep120 antibody. B.S. and D.P.M. prepared cells for FACS. H.S. designed and supervised the liquid chromatography-tandem mass spectrometry (LC-MS/MS) experiment; C.K. did the experiments, analysis, and processing; and T.R. assisted with initial analysis. E.F.F. performed the final bioinformatic analysis. F.C.A. and D.P.M. prepared the manuscript with input from all the authors.

DECLARATION OF INTERESTS

The authors declare no competing interests.

Received: February 4, 2021
Revised: December 27, 2021
Accepted: March 24, 2022
Published: April 19, 2022

REFERENCES

Adler, C.E., Fetter, R.D., and Bargmann, C.I. (2006). UNC-6/Netrin induces neuronal asymmetry and defines the site of axon formation. Nat. Neurosci. 9, 511–518.

Ahmad, F.J., Joshi, H.C., Centonze, V.E., and Baas, P.W. (1994). Inhibition of microtubule nucleation at the neuronal centrosome compromises axon growth. Neuron *12*, 271–280.

Andersen, E.F., and Halloran, M.C. (2012). Centrosome movements in vivo correlate with specific neurite formation downstream of LIM homeodomain transcription factor activity. Development *139*, 3590–3599.

Arimura, N., and Kaibuchi, K. (2007). Neuronal polarity: from extracellular signals to intracellular mechanisms. Nat. Rev. Neurosci. *8*, 194–205.

Arregui, C., Busciglio, J., Caceres, A., and Barra, H.S. (1991). Tyrosinated and detyrosinated microtubules in axonal processes of cerebellar macroneurons grown in culture. J. Neurosci. Res. *28*, 171–181.

Baas, P.W., Rao, A.N., Matamoros, A.J., and Leo, L. (2016). Stability properties of neuronal microtubules. Cytoskeleton (Hoboken) *73*, 442–460.

Bertling, E., Englund, J., Minkeviciene, R., Koskinen, M., Segerstrale, M., Castren, E., Taira, T., and Hotulainen, P. (2016). Actin tyrosine-53-phosphorylation in neuronal maturation and synaptic plasticity. J. Neurosci. *36*, 5299–5313.

Betleja, E., Nanjundappa, R., Cheng, T., and Mahjoub, M.R. (2018). A novel Cep120-dependent mechanism inhibits centriole maturation in quiescent cells. Elife *7*, e35439.

Booth, D.G., Hood, F.E., Prior, I.A., and Royle, S.J. (2011). A TACC3/ch-TOG/clathrin complex stabilises kinetochore fibres by inter-microtubule bridging. EMBO J. *30*, 906–919.

Bradke, F., and Dotti, C.G. (1999). The role of local actin instability in axon formation. Science *283*, 1931–1934.

Calderon de Anda, F., Gartner, A., Tsai, L.H., and Dotti, C.G. (2008). Pyramidal neuron polarity axis is defined at the bipolar stage. J. Cell Sci. *121*, 178–185.

Conde, C., and Caceres, A. (2009). Microtubule assembly, organization and dynamics in axons and dendrites. Nat. Rev. Neurosci. *10*, 319–332.

de Anda, F.C., Meletis, K., Ge, X., Rei, D., and Tsai, L.H. (2010). Centrosome motility is essential for initial axon formation in the neocortex. J. Neurosci. *30*, 10391–10406.

de Anda, F.C., Pollarolo, G., Da Silva, J.S., Camoletto, P.G., Feiguin, F., and Dotti, C.G. (2005). Centrosome localization determines neuronal polarity. Nature *436*, 704–708.

Distel, M., Hocking, J.C., Volkmann, K., and Koster, R.W. (2010). The centrosome neither persistently leads migration nor determines the site of axonogenesis in migrating neurons in vivo. J. Cell Biol. *191*, 875–890.

Dotti, C.G., Sullivan, C.A., and Banker, G.A. (1988). The establishment of polarity by hippocampal neurons in culture. J. Neurosci. *8*, 1454–1468.

Erdogan, B., Cammarata, G.M., Lee, E.J., Pratt, B.C., Francl, A.F., Rutherford, E.L., and Lowery, L.A. (2017). The microtubule plus-end-tracking protein TACC3 promotes persistent axon outgrowth and mediates responses to axon guidance signals during development. Neural Dev. *12*, 3.

Ferreira, A., and Caceres, A. (1989). The expression of acetylated microtubules during axonal and dendritic growth in cerebellar macroneurons which develop in vitro. Brain Res. Dev. Brain Res. *49*, 205–213.

Furey, C., Jovasevic, V., and Walsh, D. (2020). TACC3 regulates microtubule plus-end dynamics and cargo transport in interphase cells. Cell Rep. *30*, 269–283.e6.

Geraldo, S., Khanzada, U.K., Parsons, M., Chilton, J.K., and Gordon-Weeks, P.R. (2008). Targeting of the F-actin-binding protein drebrin by the microtubule plus-tip protein EB3 is required for neuritogenesis. Nat. Cell Biol. *10*, 1181–1189.

Gergely, F., Karlsson, C., Still, I., Cowell, J., Kilmartin, J., and Raff, J.W. (2000). The TACC domain identifies a family of centrosomal proteins that can interact with microtubules. Proc. Natl. Acad. Sci. U S A *97*, 14352–14357.

Guha, S., Patil, A., Muralidharan, H., and Baas, P.W. (2021). Mini-review: microtubule sliding in neurons. Neurosci. Lett. *753*, 135867.

Hammond, J.W., Huang, C.F., Kaech, S., Jacobson, C., Banker, G., and Verhey, K.J. (2010). Posttranslational modifications of tubulin and the polarized transport of kinesin-1 in neurons. Mol. Biol. Cell *21*, 572–583.

He, Y., Francis, F., Myers, K.A., Yu, W., Black, M.M., and Baas, P.W. (2005). Role of cytoplasmic dynein in the axonal transport of microtubules and neurofilaments. J. Cell Biol. *168*, 697–703.

Higginbotham, H.R., and Gleeson, J.G. (2007). The centrosome in neuronal development. Trends Neurosci. *30*, 276–283.

Jacobson, C., Schnapp, B., and Banker, G.A. (2006). A change in the selective translocation of the Kinesin-1 motor domain marks the initial specification of the axon. Neuron *49*, 797–804.

Jaqaman, K., Loerke, D., Mettlen, M., Kuwata, H., Grinstein, S., Schmid, S.L., and Danuser, G. (2008). Robust single-particle tracking in live-cell time-lapse sequences. Nat. Methods *5*, 695–702.

Joseph, N., Al-Jassar, C., Johnson, C.M., Andreeva, A., Barnabas, D.D., Freund, S.M.V., Gergely, F., and Van Breugel, M. (2018). Disease-associated mutations in CEP120 destabilize the protein and impair ciliogenesis. Cell Rep. *23*, 2805–2818.

Kinoshita, K., Noetzel, T.L., Pelletier, L., Mechtler, K., Drechsel, D.N., Schwager, A., Lee, M., Raff, J.W., and Hyman, A.A. (2005). Aurora A phosphorylation of TACC3/maskin is required for centrosome-dependent microtubule assembly in mitosis. J. Cell Biol. *170*, 1047–1055.

Komarova, Y., De Groot, C.O., Grigoriev, I., Gouveia, S.M., Munteanu, E.L., Schober, J.M., Honnappa, S., Buey, R.M., Hoogenraad, C.C., Dogterom, M., et al. (2009). Mammalian end binding proteins control persistent microtubule growth. J. Cell Biol. *184*, 691–706.

Konishi, Y., and Setou, M. (2009). Tubulin tyrosination navigates the kinesin-1 motor domain to axons. Nat. Neurosci. *12*, 559–567.

Kuijpers, M., and Hoogenraad, C.C. (2011). Centrosomes, microtubules and neuronal development. Mol. Cell. Neurosci. *48*, 349–358.

Lefcort, F., and Bentley, D. (1989). Organization of cytoskeletal elements and organelles preceding growth cone emergence from an identified neuron in situ. J. Cell Biol. *108*, 1737–1749.

Liao, Y., Wang, J., Jaehnig, E.J., Shi, Z., and Zhang, B. (2019). WebGestalt 2019: gene set analysis toolkit with revamped UIs and APIs. Nucleic Acids Res. *47*, W199–W205.

Matov, A., Applegate, K., Kumar, P., Thoma, C., Krek, W., Danuser, G., and Wittmann, T. (2010). Analysis of microtubule dynamic instability using a plus-end growth marker. Nat. Methods *7*, 761–768.

McAlister, G.C., Nusinow, D.P., Jedrychowski, M.P., Wuhr, M., Huttlin, E.L., Erickson, B.K., Rad, R., Haas, W., and Gygi, S.P. (2014). MultiNotch MS3 enables accurate, sensitive, and multiplexed detection of differential expression across cancer cell line proteomes. Anal. Chem. *86*, 7150–7158.

Meka, D.P., Scharrenberg, R., Zhao, B., Kobler, O., Konig, T., Schaefer, I., Schwanke, B., Klykov, S., Richter, M., Eggert, D., et al. (2019). Radial somatic F-actin organization affects growth cone dynamics during early neuronal development. EMBO Rep. *20*, e47743.

Merriam, E.B., Millette, M., Lumbard, D.C., Saengsawang, W., Fothergill, T., Hu, X., Ferhat, L., and Dent, E.W. (2013). Synaptic regulation of microtubule dynamics in dendritic spines by calcium, F-actin, and drebrin. J. Neurosci. *33*, 16471–16482.

Mortuza, G.B., Cavazza, T., Garcia-Mayoral, M.F., Hermida, D., Peset, I., Pedrero, J.G., Merino, N., Blanco, F.J., Lyngso, J., Bruix, M., et al. (2014). XTACC3-XMAP215 association reveals an asymmetric interaction promoting microtubule elongation. Nat. Commun. *5*, 5072.

Namba, T., Kibe, Y., Funahashi, Y., Nakamuta, S., Takano, T., Ueno, T., Shimada, A., Kozawa, S., Okamoto, M., Shimoda, Y., et al. (2014). Pioneering axons regulate neuronal polarization in the developing cerebral cortex. Neuron *81*, 814–829.

Nanjundappa, R., Kong, D., Shim, K., Stearns, T., Brody, S.L., Loncarek, J., and Mahjoub, M.R. (2019). Regulation of cilia abundance in multiciliated cells. Elife *8*, e44039.

Neukirchen, D., and Bradke, F. (2011). Cytoplasmic linker proteins regulate neuronal polarization through microtubule and growth cone dynamics. J. Neurosci. *31*, 1528–1538.

Noctor, S.C., Martinez-Cerdeno, V., Ivic, L., and Kriegstein, A.R. (2004). Cortical neurons arise in symmetric and asymmetric division zones and migrate through specific phases. Nat. Neurosci. *7*, 136–144.

Nwagbara, B.U., Faris, A.E., Bearce, E.A., Erdogan, B., Ebbert, P.T., Evans, M.F., Rutherford, E.L., Enzenbacher, T.B., and Lowery, L.A. (2014). TACC3 is a microtubule plus end-tracking protein that promotes axon elongation and also regulates microtubule plus end dynamics in multiple embryonic cell types. Mol. Biol. Cell *25*, 3350–3362.

Pollarolo, G., Schulz, J.G., Munck, S., and Dotti, C.G. (2011). Cytokinesis remnants define first neuronal asymmetry in vivo. Nat. Neurosci. *14*, 1525–1533.

Powell, S.K., Rivas, R.J., Rodriguez-Boulan, E., and Hatten, M.E. (1997). Development of polarity in cerebellar granule neurons. J. Neurobiol. *32*, 223–236.

Randlett, O., Poggi, L., Zolessi, F.R., and Harris, W.A. (2011). The oriented emergence of axons from retinal ganglion cells is directed by laminin contact in vivo. Neuron *70*, 266–280.

Rao, A.N., Patil, A., Black, M.M., Craig, E.M., Myers, K.A., Yeung, H.T., and Baas, P.W. (2017). Cytoplasmic dynein transports axonal microtubules in a polarity-sorting manner. Cell Rep. *19*, 2210–2219.

Reed, N.A., Cai, D., Blasius, T.L., Jih, G.T., Meyhofer, E., Gaertig, J., and Verhey, K.J. (2006). Microtubule acetylation promotes kinesin-1 binding and transport. Curr. Biol. *16*, 2166–2172.

Rivas, R.J., and Hatten, M.E. (1995). Motility and cytoskeletal organization of migrating cerebellar granule neurons. J. Neurosci. *15*, 981–989.

Sakakibara, A., Sato, T., Ando, R., Noguchi, N., Masaoka, M., and Miyata, T. (2014). Dynamics of centrosome translocation and microtubule organization in neocortical neurons during distinct modes of polarization. Cereb. Cortex *24*, 1301–1310.

Sanchez-Huertas, C., Freixo, F., Viais, R., Lacasa, C., Soriano, E., and Luders, J. (2016). Non-centrosomal nucleation mediated by augmin organizes microtubules in post-mitotic neurons and controls axonal microtubule polarity. Nat. Commun. *7*, 12187.

Schaar, B.T., and McConnell, S.K. (2005). Cytoskeletal coordination during neuronal migration. Proc. Natl. Acad. Sci. U S A *102*, 13652–13657.

Shoukimas, G.M., and Hinds, J.W. (1978). The development of the cerebral cortex in the embryonic mouse: an electron microscopic serial section analysis. J. Comp. Neurol. *179*, 795–830.

Sironi, L., Solon, J., Conrad, C., Mayer, T.U., Brunner, D., and Ellenberg, J. (2011). Automatic quantification of microtubule dynamics enables RNAi-screening of new mitotic spindle regulators. Cytoskeleton (Hoboken) *68*, 266–278.

Slaughter, T., Wang, J., and Black, M.M. (1997). Microtubule transport from the cell body into the axons of growing neurons. J. Neurosci. *17*, 5807–5819.

Stepanova, T., Slemmer, J., Hoogenraad, C.C., Lansbergen, G., Dortland, B., De Zeeuw, C.I., Grosveld, F., Van Cappellen, G., Akhmanova, A., and Galjart, N. (2003). Visualization of microtubule growth in cultured neurons via the use of EB3-GFP (end-binding protein 3-green fluorescent protein). J. Neurosci. *23*, 2655–2664.

Stiess, M., Maghelli, N., Kapitein, L.C., Gomis-Ruth, S., Wilsch-Brauninger, M., Hoogenraad, C.C., Tolic-Norrelykke, I.M., and Bradke, F. (2010). Axon extension occurs independently of centrosomal microtubule nucleation. Science *327*, 704–707.

Szklarczyk, D., Gable, A.L., Lyon, D., Junge, A., Wyder, S., Huerta-Cepas, J., Simonovic, M., Doncheva, N.T., Morris, J.H., Bork, P., et al. (2019). STRING v11: protein-protein association networks with increased coverage, supporting functional discovery in genome-wide experimental datasets. Nucleic Acids Res. *47*, D607–D613.

Tinevez, J.Y., Perry, N., Schindelin, J., Hoopes, G.M., Reynolds, G.D., Laplantine, E., Bednarek, S.Y., Shorte, S.L., and Eliceiri, K.W. (2017). TrackMate: an open and extensible platform for single-particle tracking. Methods *115*, 80–90.

Tsai, J.J., Hsu, W.B., Liu, J.H., Chang, C.W., and Tang, T.K. (2019). CEP120 interacts with C2CD3 and Talpid3 and is required for centriole appendage assembly and ciliogenesis. Sci. Rep. *9*, 6037.

Tsai, L.H., and Gleeson, J.G. (2005). Nucleokinesis in neuronal migration. Neuron *46*, 383–388.

von Mering, C., Huynen, M., Jaeggi, D., Schmidt, S., Bork, P., and Snel, B. (2003). STRING: a database of predicted functional associations between proteins. Nucleic Acids Res. *31*, 258–261.

Witte, H., Neukirchen, D., and Bradke, F. (2008). Microtubule stabilization specifies initial neuronal polarization. J. Cell Biol. *180*, 619–632.

Wloga, D., Joachimiak, E., and Fabczak, H. (2017). Tubulin post-translational modifications and microtubule dynamics. Int. J. Mol. Sci. *18*, 2207.

Xie, Z., Moy, L.Y., Sanada, K., Zhou, Y., Buchman, J.J., and Tsai, L.H. (2007). Cep120 and TACCs control interkinetic nuclear migration and the neural progenitor pool. Neuron *56*, 79–93.

Yao, R., Kondoh, Y., Natsume, Y., Yamanaka, H., Inoue, M., Toki, H., Takagi, R., Shimizu, T., Yamori, T., Osada, H., and Noda, T. (2014). A small compound targeting TACC3 revealed its different spatiotemporal contributions for spindle assembly in cancer cells. Oncogene *33*, 4242–4252.

Yu, W., and Baas, P.W. (1994). Changes in microtubule number and length during axon differentiation. J. Neurosci. *14*, 2818–2829.

Zhao, B., Meka, D.P., Scharrenberg, R., Konig, T., Schwanke, B., Kobler, O., Windhorst, S., Kreutz, M.R., Mikhaylova, M., and Calderon De Anda, F. (2017). Microtubules modulate F-actin dynamics during neuronal polarization. Sci. Rep. *7*, 9583.

Zmuda, J.F., and Rivas, R.J. (1998). The Golgi apparatus and the centrosome are localized to the sites of newly emerging axons in cerebellar granule neurons *in vitro*. Cell Motil Cytoskeleton *41*, 18–38.

Zolessi, F.R., Poggi, L., Wilkinson, C.J., Chien, C.B., and Harris, W.A. (2006). Polarization and orientation of retinal ganglion cells *in vivo*. Neural Dev. *1*, 2.

STAR★METHODS

KEY RESOURCES TABLE

REAGENT or RESOURCE	SOURCE	IDENTIFIER
Antibodies		
Mouse anti-acetylated Tubulin	Sigma	Cat# T7451; RRID:AB_609894
Rat anti-α-Tubulin	SySy	Cat# 302217; RRID:AB_314247
Mouse anti-Ankyrin G (463)	Santa Cruz	Cat# sc-12719; RRID:AB_626674
Mouse anti-Arl13b	BioLegend	Cat# N295B/66; RRID:AB_2877361
Guinea pig anti-βIII-Tubulin	SySy	Cat# 302304; RRID:AB_10805138
Rabbit anti-Cep120	this manuscript	N/A
Mouse anti-GAPDH	Santa Cruz	Cat# sc-32233; RRID:AB_627679
Rabbit anti-Pericentrin	Covance	Cat# PRB-432C; RRID:AB_2313709
Mouse anti-polyglutamylated Tubulin	Sigma	Cat# T9822; RRID:AB_477598
Mouse anti-SMI 31	BioLegend	Cat# 801601; RRID:AB_2564641
Rabbit anti-TACC3	Cell Signaling	Cat# 8069; RRID:AB_10830219
Mouse anti-Tau-1	Millipore	Cat# MAB3420; RRID:AB_11213630
Rat anti-tryosinated Tubulin (YL1/2)	Abcam	Cat# ab6160; RRID:AB_305328
Sheep anti-Tubulin (total)	Cytoskeleton	Cat# ATN02; RRID:AB_10708807
anti-guinea pig goat IgG AF647	Invitrogen	Cat# A21450; RRID:AB_141882
anti-mouse goat IgG HRP	Dianova	Cat# 115-035-003: AB_10015289
anti-mouse donkey IgG AF 488	Invitrogen	Cat# A21202; RRID:AB_141607
anti-mouse goat IgG STAR 580	Abberior	Cat# 2-0002-500-1; RRID:AB_228307
anti-mouse donkey IgG AF 647	Invitrogen	Cat# A31571; RRID:AB_162542
anti-rabbit goat IgG AF 488	Invitrogen	Cat# A11077; ; RRID:AB_2534121
anti-rabbit goat IgG HRP	Dianova	Cat# 111-035-003; RRID: AB_2313567
anti-rabbit donkey IgG AF 647	Invitrogen	Cat# A31573; RRID:AB_2536183
anti-rat donkey IgG HRP	Dianova	Cat# 712-035-153; RRID:AB_2340639
anti-rat goat IgG AF 568	Invitrogen	Cat# A11077; RRID:AB_2534121
anti-rat goat IgG STAR RED	Abberior	Cat# STRED-1007-500UG
anti-sheep donkey IgG HRP	Dianova	Cat# 713-035-147; RRID:AB_2340710
anti-sheep donkey IgG STAR RED	Abberior	Cat# STRED-1056-500UG
Chemicals, peptides, and recombinant proteins		
Hoechst dye	Invitrogen	Cat# 33258; RRID:AB_2651133
Cytochalasin D	Sigma	Cat# C2618-200UL
Taxol	Sigma	Cat# T7402
Nocodazole	Sigma	Cat# M1404-10MG
Spindlactone B	Axon Medchem	Cat# 2474
TMT10plex™ Reagent Set for Isobar Marking	Thermo Scientific	Cat# 90110
Deposited data		
Data related to Figures 2, 3, 6, and S7	Mendeley data	https://doi.org/10.17632/cvk3nf2mpr.1
Experimental models: Cell lines		
BL21-CodonPlus (De3)-RIL competent cells	Agilent Technologies	cat# 230280
Experimental models: Organisms/strains		
Mice; C57BL6J	Jackson	https://www.jax.org
Rats; HsdCpb:WU (all rat cultures otherwise mentioned)	Envigo	https://www.envigo.com

(*Continued on next page*)

Continued

REAGENT or RESOURCE	SOURCE	IDENTIFIER
Rats; HanRj:WI (Figures 3A and 3B)	Janvier	https://www.janvier-labs.com
Recombinant DNA		
CAG-Venus	a gift from Zhigang Xie; de Anda et al., 2010	N/A
pSilencer2-U6-shControl	Xie et al., (2007)	N/A
pSilencer2-U6-shCep120	Xie et al., (2007)	N/A
pAAV-CAG-tDimer	a gift from Thomas Oertner	N/A
CMV-EB3-tdTomato	a gift from Erik Dent (via Addgene); Merriam et al., (2013)	RRID:Addgene_50708
CMV- Actin-mCherry	a gift from Pirta Hotulainen; Bertling et al., (2016)	N/A
pBrain-GFP-TACC3KDP-shTACC3	a gift from Stephen Royle (via Addgene); Booth et al., (2011)	RRID:Addgene_59356
pBrain-GFP-shGL2	a gift from Stephen Royle (via Addgene); Booth et al., (2011)	RRID:Addgene_60004
pBrain-GFP-shTACC3	a gift from Stephen Royle (via Addgene); Booth et al., (2011)	RRID:Addgene_59355
CMV-GFP-TACC3	a gift from Stephen Royle (via Addgene); Booth et al., (2011)	RRID:Addgene_59356
CMV-tdTomato-TACC3	This manuscript	N/A
CAG-Farnesylated-GFP	a gift from Annette Gärtner; de Anda et al., 2010	N/A
pNeuroD-GFP	a gift from Zhigang Xie; de Anda et al., 2010	N/A
pET-21a	Novagen	Cat# 69740-3
Software and algorithms		
Fiji	Max-Planck-Gesellschaft	http://fiji.sc/; RRID: SCR_002285
ImageJ	NIH	https://imagej.net/; RRID:SCR_003070
Graphpad Prism versions 8 and 9	GraphStats	https://www.graphpad.com/; RRID: SCR_002798
Adobe Illustrator	Adobe	https://www.adobe.com/products/illustrator.html; RRID: SCR_014198
Huygens Professional	Scientific Volume Imaging	RRID: SCR_014237

RESOURCE AVAILABILITY

Lead contact

Further information and requests for resources and reagents should be directed to and will be fulfilled by the lead contact, Froylan Calderon de Anda (froylan.calderon@zmnh.uni-hamburg.de).

Materials availability

Cep 120 antibody and tdTomato-TACC3 plasmids, the reagents generated for this paper, are shared by the lead contact upon request. Note: Cep120 antibody sharing is subjected to availability.

Data and code availability

- All data reported in this paper will be shared by the lead contact upon request.
- This paper does not report original code.
- Any additional information required to reanalyze the data reported in this paper is available from the lead contact upon request.

EXPERIMENTAL MODEL AND SUBJECT DETAILS

Animal experiments

All rat (Wistar) and mouse (C57Bl6J) experiments were performed according to the German and European Animal Welfare Act and with the approval of local authorities of the city-state Hamburg (Behörde für Gesundheit und Verbraucherschutz, Fachbereich Veterinärwesen) as well as the animal care committee of the University Medical Center Hamburg-Eppendorf and the

Lower Saxony State Office for Consumer Protection and Food Safety (Niedersächsisches Landesamt für Verbraucherschutz und Lebensmittelsicherheit), as well as the Zentralen Tierexperimentellen Einrichtung (ZTE) of the Universitätsmedizin Göttingen (UMG). Pregnant rats and mice, 2-4 months old, used for primary cultures. PrimmBiotech, Inc generated Cep 120 antibody by immunizing New Zealand white rabbits from Charles River.

Cellular models

Primary Rat hippocampal and mouse cortical cultures, and BL21-CodonPlus (De3)-RIL competent cells (Agilent Technologies, cat. # 230280).

METHOD DETAILS

RNAi and fluorescent protein constructs

We previously reported the Venus, Farnesylated-GFP, pNeuroD-GFP, control shRNA, Cep 120 shRNA, and Cep 120-GFP plasmids (de Anda et al., 2010; Xie et al., 2007). tDimer (pAAV-CAG-tDimer) was kindly provided by Thomas Oertner (ZMNH, UKE). EB3-tdTomato was a gift from Erik Dent (Addgene plasmid # 50708; http://n2t.net/addgene:50708; RRID:Addgene_50708 (Merriam et al., 2013)), pBrain-GFP-shTACC3 was a gift from Stephen Royle (Addgene plasmid # 59355; http://n2t.net/addgene:59355; RRID: Addgene_59355 (Booth et al., 2011)), pBrain-GFP-shGL2 was a gift from Stephen Royle (Addgene plasmid # 60004; http://n2t.net/addgene:60004; RRID:Addgene_60004 (Booth et al., 2011)). Actin-mCherry plasmid, a gift from Pirta Hotulainen (Minerva Foundation Institute for Medical Research, Helsinki, Finland) (Bertling et al., 2016).

Generation of tdTomato-TACC3 plasmid (pCMV-tdTomato-TACC3): GFP-TACC3 from pBrain-GFP-TACC3KDP-shTACC3 (a gift from Stephen Royle, Addgene plasmid # 59356; http://n2t.net/addgene:59356; RRID: Addgene_59356 (Booth et al., 2011)) was inserted into the Addgene plasmid # 50708 (with EB3 insert in tdTomato-N1 backbone) by restriction cloning at the NheI and MfeI restriction sites, thus creating GFP-TACC3 plasmid. Next, the GFP tag is replaced with tdTomato (from Addgene plasmid # 50708, EB3 insert in tdTomato-N1 backbone) at unique AgeI and BrsGI restriction sites to create tdTomato-TACC3 plasmid.

In utero electroporation (IUE)

Pregnant C57BL/6 mice with E13 or E15 embryos were first administered with pre-operative analgesic, buprenorphine (0.1 mg/kg), by subcutaneous injection. After 30 min, mice were anesthetized with isoflurane (4% for induction, 2–3% for maintenance) in oxygen (0.5–0.8 L/min for induction and maintenance). Later, uterine horns were exposed, and plasmids mixed with Fast Green (Sigma) were microinjected into the lateral ventricles of embryos. Five current pulses (50 ms pulse/950 ms interval) at 30V for E13 and 35V for E15 were delivered across the heads of embryos. After surgery, mice were kept in a warm environment and were provided with moist food containing post-operative analgesic, meloxicam (0.2–1 mg/kg), until they were euthanized for collection of the brains from the embryos. The brains were either used for cortical cultures or cortical slices or FACS.

Mouse primary cortical cultures

Brain cortices transfected via IUE at E13 or E15 with control or Cep120 shRNA or Cep120-GFP or TACC3 shRNA or GL2 shRNA plasmids in combination with tDimer or EB3-tdTomato or Venus alone were used for cortical cultures. The concentration of shRNA (control or Cep120 shRNA or TACC3 shRNA, GL2 shRNA), Cep120 GFP plasmids injected was 2-3-fold higher than that of the tDimer plasmids or EB3-tdTomato. We used 1.5 μg/μL for shRNA (control or Cep120 shRNA or TACC3 shRNA), 1.2 μg/μL Cep120-GFP, 0.5 μg/μL of tDimer or EB3-tdTomato and 0.5 μg/μL of Venus plasmid. Two days later pregnant mice were anesthetized with CO2/O2, euthanized before taking the E17 embryos out from their uteri. Embryos were then decapitated, skulls were opened, brains were collected in petri dishes with Hibernate-E medium (Invitrogen) on ice. Hemispheres were separated, meninges were carefully stripped away, and cortices were dissected on ice. Transfected (fluorescent) cortical regions were identified and dissected on ice under a stereo microscope (Olympus SZX16) equipped with a UV light source. The isolated cortical regions were first incubated in 1x HBSS (Invitrogen) with papain and DNase (Worthington) for 10 min at 37°C neurons and then triturated. The cells were then pelleted and washed with fresh HBSS before they were plated on poly-L-lysine coated coverslips or tissue culture chambers (Sarstedt, for live-imaging) in Neurobasal/B27 medium (Invitrogen), maintained in culture for 24 to 72h at 37°C with 5% CO2 before use.

Mouse cortical slices

We introduced Cep120 shRNA or control shRNA or Cep120-GFP plasmids in combination with tDimer plasmid into brain cortices at E15. We used 1.5 μg/μL for shRNA (control or Cep120 shRNA), 1.2 μg/μL of Cep120-GFP and 0.5 μg/μL of tDimer. The brains collected from E19 embryos were post-fixed in 4% paraformaldehyde (PFA) overnight at 4°C and later moved to 30% sucrose (in PBS) until they were completely sunk. Brains were then embedded in Tissue Tek OCT compound and stored at 80°C until they were sectioned to 60 μm slices using a cryostat.

Rat primary hippocampal neuron cultures and transfections

Pregnant rats were anesthetized with CO2/O2, euthanized before taking the E18 embryos out from their uteri. Embryos were then decapitated, skulls were opened, brains were collected in petri dishes with HBSS on ice. Hemispheres were separated, meninges

were carefully stripped away, and hippocampi were dissected on ice and triturated in 1xHBSS (Invitrogen) after digestion by papain and DNase (Worthington for 10 min at 37°C). Transfections were performed using the Amaxa nucleofector system following the manufacturer's manual. The final concentration for the EB3-tdTomato or Farnesylated-GFP plasmid was 1 μg, for tdTomato-TACC3 we used 0.3 or 0.5 μg. Empty pcDNA 3.1 was used to make up to 3 μg of DNA for 5 × 10^6 cells per each transfection mix as per the manufacturer recommendation. After electroporation, neurons were plated on poly-L-lysine coated coverslips or tissue culture chambers (Sarstedt, for live-imaging) in Neurobasal/B27 medium (Invitrogen) and were maintained in culture for 24 to 72h or 7-8 days at 37°C with 5% CO2 before use.

Pharmacological treatments

Rat hippocampal or mouse cortical neurons in culture were treated with CytoD (Sigma, #C2618-200UL) - 2μM or Taxol (Sigma, #T7402) - 5nM, either at the time of plating (at 0h) or ~28 to 30h later.

Mouse cortical neurons were treated for 30min with 6 μM Nocodazole (Sigma, M1404-10MG) 48h after plating. Mouse cortical neurons were treated with Spindlactone B (SPL-B; a TACC3 inhibitor; Axon Medchem #2474) – 0.25 μg per ml, at the time of plating (at 0h) cells were then PFA (4%) fixed after 48 or 72h in culture for immunostaining.

Cep120 antibody generation

The rabbit anti-Cep120 polyclonal antibody was generated as previously described (Nanjundappa et al., 2019). Briefly, a C-terminal fragment of the mouse Cep120 gene (amino acids 860-988) was PCR amplified and subcloned into pET-21a (+) vector (Novagen, cat. # 69740-3) at unique NdeI and XhoI sites. Soluble recombinant Cep120-His6 protein was expressed in BL21-CodonPlus (De3)-RIL competent cells (Agilent Technologies, cat. # 230280) and purified on HisPurTM Cobalt Resin (Pierce, cat. # 89964) following manufacturer's protocols. 8 mg of antigen was used to inject three New Zealand white rabbits (done by PrimmBiotech, Inc.). Serum from two of the animals (SCA/14-R2 and SCA/14-R3) showed specificity for Cep120, one of them tested on cells and tissues, as previously described (Nanjundappa et al., 2019). In this manuscript we used antibodies from SCA/14-R2.

Immunofluorescence

Rat hippocampal or mouse cortical neurons grown on coverslips were fixed either with 4% paraformaldehyde (PFA) at 37°C for 10 min or with 4% paraformaldehyde (PFA) at 37°C for 2 min, followed by 3 min ice cold Methanol incubation at −20°C. Cells were then permeabilized with 0.5% Triton X-100 for 10 min. Non-specific binding was blocked by incubation with 5% donkey serum in PBS for 60 min at RT (room temperature), followed by specific primary antibody incubation Table S1180 min at RT or overnight at 4°C, followed by 3 times 4 min PBS washes. Coverslips were incubated with respective anti-mouse or anti-rabbit Alexa Fluor 488 or 568 or 647 secondary antibodies Table S2, along with Hoechst dye (1:10,000, Invitrogen # 33258) to stain for nuclei for 60 min at RT followed by three washing steps with PBS. Coverslips were mounted onto slides using Fluoromount-G® (SouthernBiotech) and were stored protected from light.

Antibodies used for immunostainings: Primary -mouse anti-AcetyTub, 1:700 (Sigma T7451); rat anti-α-tubulin, 1:400 (SySy 302217); mouse anti-Ankyrin G (463), 1:700 (Santa Cruz sc-12719); mouse anti-Arl13b, 1:200 (BioLegend N295B/66); guinea pig anti-βIII-tubulin, 1:2000 (SySy 302304); rabbit anti-Cep120, 1:800 (lab-made); rabbit anti-Pericentrin, 1:500 (Covance PRB-432C); mouse anti-PolyGluTub, 1:250 (Sigma T9822); mouse anti-SMI 31, 1:300 (BioLegend 801601); rabbit anti-TACC3, 1:200 (Cell Signaling 8069); mouse anti-Tau-1, 1:700 (Millipore MAB3420); rat anti-Tryosinated tubulin (YL1/2), 1:400 (Abcam ab6160); sheep anti-tubulin (total), 1:400 (Cytoskeleton ATN02). Secondary – goat anti-guinea pig IgG AF 647, 1:1000 (Invitrogen A21450); donkey anti-mouse IgG AF 488, 1:1000 (Invitrogen A21202); goat anti-mouse IgG STAR 580, 1:500 (Abberior 2-0002-500-1); donkey anti-mouse IgG AF 647, 1:1000 (Invitrogen A31571); goat anti-rabbit IgG AF 488, 1:1000 (Invitrogen A11077); donkey anti-rabbit IgG AF 647, 1:1000 (Invitrogen A31573); goat anti-rat IgG AF 568, 1:1000 (Invitrogen A11077); goat anti-rat IgG STAR RED, 1:500 (Abberior STED-1007-500UG); donkey anti-sheep IgG STAR RED, 1:400 (Abberior STED-1056-500UG).

Epifluorescence imaging

Imaging was performed on an inverted Nikon microscope (Eclipse, Ti) with a 60× oil immersion objective (NA 1.4). During time-lapse imaging, cells plated on 4 well culture chambers (Sarstedt or Ibidi) were kept in an acrylic chamber at 37°C in 5% CO2. Light intensity of each channel was set at 4, with an exposure time of 300 ms and frame interval of 2 s for 5min. For imaging fixed cells imaging, light intensity of each channel was set at 1, with an exposure time of 100-900 ms for all the fluorophores except for Hoechst dye (5ms). Images were captured with a CoolSNAP HQ2camera (Roper Scientific) using NIS-Elements AR software (version 4.20.01 from Nikon Corporation).

Long-term live-imaging

For long-lasting time-lapse experiments, neurons were stored in an automated incubator/imaging system (Cytation™ 5 Cell Imaging Multi-Mode Reader associated with a BioSpa™ 8 Automated Incubator, BioTek, USA). The plates were stored in the BioSpa at 37°C and 5% CO_2 and were automatically transferred to the Cytation™ 5 for imaging. For all live-imaging experiments a 20X Plan 0.45 NA objective was used and several fields of view were acquired in time-lapse mode using the point-visiting function.

STED microscopy and deconvolution

All STED z-stacks were acquired on a *Leica* TCS SP8 gated STED system (*Leica microsystems, Manheim, Germany*) equipped with a pulsed 775 nm depletion laser and a pulsed white light laser (WLL) for excitation. For acquiring images, either a *Leica* Objective HC APO CS2 100×/1.40 Oil or a Glycerol objective (*Leica,* HC APO 93x/1.30 GLYC motCORR) were used.

Rat hippocampal neurons co-labelled with Primary antibodies - mouse anti-AcetyTub 1:400 (Sigma T7451); rat anti-α-tubulin 1:250 (SySy 302217); mouse anti-PolyGluTub 1:250 (Sigma T9822); rat anti-tryosinated tubulin (YL1/2), 1:400 (Abcam ab6160), followed by species specific secondary antibodies, goat anti-mouse IgG STAR 580, 1:200 (Abberior 2-0002-500-1); goat anti-rat IgG STAR RED, 1:200 (Abberior STED-1007-500UG); donkey anti-sheep IgG STAR RED, 1:200 (Abberior STED-1056-500UG), were embedded in Mowiol or Aberrior liquid Mount and excited via the WLL at 640, 561 and 488nm, respectively. Emission was acquired between 650 and 710nm for Abberior Star RED and 580–620nm for Abberior Star 580 and 500–530nm for AF 488. STED channels. Abberior Star RED and Star 580 were depleted with 50% and 100% with 775 nm depletion laser, respectively. The detector time gates for both channels were set to 0.5– 6ns. The imaging format for all images was set to 2048 × 2048 and an optical zoom of 3 resulted in a pixel size for oil: x/y 18,9nm, for glycerol: x/y 20,4nm. Z spacing was set to 120nm or 160nm. Scan speed was set to 600 lines per second and 8-times line averaging was applied. Confocal overview images were acquired with the same objective, same optical settings but less zoom, less averaging and less excitation power.

Deconvolution of STED z-stacks were done with Huygens Professional (*Scientific Volume Imaging, Hilversum, The Netherlands*). Within the *Deconvolution wizard*, images were subjected to automatic background correction (*lowest* value method), *Signal-to-noise ratio* was set to 15 for both channels and the *Optimized iteration mode of the CMLE* was applied until the algorithm reached 25 iteration steps.

Confocal spinning disk imaging

Images were taken with 10X and 60X oil (NA 1.4) objectives on a Nikon EclipseTi2 inverted spinning disk microscope equipped with an LED light source (Lumencor® from AHF analysentechnik AG, Germany), a spinning disk confocal unit (X-Light V2 L-FOV from CrestOptics S.p.A. Italy) and a digital CMOS camera (ORCA-Flash4.0 V3 C13440-20CU from Hamamatsu) controlled with NIS-Elements software. 60X z series images with a step size of 300 nm and 1 μm for primary neurons and embryonic brain slices, respectively.

EB3 comets tracking in the soma of developing neurons

TrackMate (v6.0.1), an open-source Fiji (ImageJ) plugin (Tinevez et al., 2017) was used for the semi-automated tracking of EB3 comets from 2D epifluorescence time-lapse live-images of EB3-tdTomato expressing primary neurons. EB3-tdTomato transfected DIV1-2 rat hippocampal neurons (via Amaxa nucleofection) and DIV1 mouse cortical neurons co-transfected with EB3-tdTomato or control or Cep120 shRNA or Cep120 GFP plasmids (via IUE) were used for analysis.

Pre-processing of the EB3 time-lapse images before loading them on to TrackMate: Substract background tool in the Fiji was chosen, Rolling ball radius selection of 1 pixel delineated the EB3 comets from the background distinctively. To study the EB3 dynamics in the soma of the developing neurons, we have specifically chosen the neuronal soma area for our analysis. After loading the time-lapse to the TrackMate, LOG detector was selected, and the following parameters were given to be able to detect most but specific EB3 comets in the time-lapse: i). blob diameter was chosen to 3 pixels (∼0.45 microns), ii). threshold value between 25 and 40 (based on the signal to noise ratio). iii). Median filter and sub-pixel localization parameters were set to on. In the next step, no initial thresholding was performed and continued to Hyperstack displayer, this step detects all the comets in the 151 frames (2 frames per sec for 5min). Next, to create tracks from the EB3 comets in the time-lapse, LAP tracker (Jaqaman et al., 2008) was selected, under which the following parameters were set without featuring any penalties: a). for Frame to frame linking of the comets track, maximum distance set was to 1 micron; b). for Track segment gap closing, gap closing was allowed and maximum distance set to 1 micron with a maximum frame gap set to 2; c). Track merging was allowed when the maximum distance is 1 micron. The EB3 tracks thus created were checked one-by-one manually using the TrackScheme option. Individual tracks created in the TrackScheme and the actual EB3 comet tracks were verified manually in the time-lapse, false and non-specific tracks were edited. Using the Analysis option all the data related to the EB3 comets and tracks were obtained as.csv files from which the following parameters were analyzed to study the EB3 dynamics: 1. EB3 track speed (microns per sec); 2. Growth (displacement) of each EB3 comet per frame (microns) and 3. Total duration of each EB3 tracks (in seconds). To plot the EB3 tracks and comets dynamics near the MTOC, the XY coordinates of the MTOC for each cell is obtained through Fiji - ImageJ by identifying the XY coordinates of the EB3 asters in the time-lapses and set them to (0,0) and then the coordinates of the EB3 tracks' and comets' XY coordinates (available in the data obtained after TrackMate analysis) were normalized accordingly.

Axonal phenotype analysis

Epifluorescence 60× oil objective images of Tau-1 or SMI 31 or Ankyrin-G immunostained primary mouse cortical and rat hippocampal neurons were used. Images were loaded onto Fiji - ImageJ and Tau1/SMI 31 positive gradients in 48-72 h old neurons and Ankyrin-G rich axon initial segment (AIS) in 7-8 days old neurons, hallmarks of axonal identities, were manually quantified.

Fluorescent intensity measurements

Images acquired on STED (TyrTub and AcetyTub immunostainings) or confocal spinning disk (AcetyTub immunostainings) microscope were used for analysis. Images were loaded onto Fiji - ImageJ and z-projection (sum slices) for the entire stacks was performed

on the images. Using Fiji - ImageJ, soma region was carefully delineated and integrated density in the soma (soma area * mean intensity) was measured. For background correction, mean intensity (background mean intensity) was obtained from the neighboring region (out of the cell). Using the following equation, we obtained the corrected values. corrected value = integrated density in the soma – (background mean intensity * soma area).

Fluorescence signal area measurements

STED images were loaded onto Fiji - ImageJ and z-projection (Maximum intensity projections) for the stacks were created and a threshold applied by using the default setting, the min and max values were adjusted to ensure the thresholding of the fluorescent signal in the respective channels to obtain area of fluorescence signal. Soma area is carefully delineated, and area of fluorescence signal was then normalized to the soma area.

Western blotting

Rat cortical neurons were treated with 2uM CytoD and 5nM Taxol either at the time of plating (0h) or after ~28 to 30h after plating and harvested 18h after adding the compounds, 2μM CytoD or 5nM Taxol, and lysed in RIPA buffer (50mM Tris-HCl pH 7.4, 150mM NaCl, 1mM EGTA, 1% NP-40, 0.25% sodium deoxycholate, supplemented with proteinase inhibitor (Roche Mini Complete EDTA Free, Roche 11836170001) and phosphatase inhibitor (Phospho STOP, Roche 4906845001). The lysates were cleared by centrifugation 13000 rpm for 10 min at 4°C.The supernatant was transferred to ice-cold tube, and then the protein concentration in the samples was determined by the Pierce™ BCA Protein Assay Kit (Thermo Fisher Scientific, 23225) according to the manufacturer's instructions. 20 μg protein was resolved on 10-15% sodium dodecyl sulfate (SDS) polyacrylamide Tris-glycine gradient gel at 30mA/gel. Proteins from the polyacrylamide gel were transferred to a PVDF membrane (Millipore) with wet transfer method (Gels were electrophoresed at 35 V overnight at 4°C). The total amount of protein on the membranes were determined by Revert™ 700 Total Protein Stain for Western blot normalization Licor (926-11010) according to the manufacturer's instructions.

Membranes were blocked in TBS-Tween20 0.1% with 5% BSA, or with 5% non-fat dry milk powder according to the antibody's datasheet instructions for 1h at room temperature. After blocking, the membranes were incubated with primary antibodies diluted in the blocking buffer overnight at 4°C (Primary antibodies listed below). Following primary antibody incubation, membranes were washed for 30 min in 0.1% TBS-Tween20 and incubated for 2 h at RT with the respective horseradish peroxidase conjugated anti-IgG secondary antibodies (Secondary antibodies listed below) and then washed for 30 min in TBS-Tween20 0.1%. Afterward, immunoreactivity signals on the membranes were visualized by enhanced chemiluminescence NTAS, ChemoStar, ECL Imager. Western blots were analyzed using Fiji software. Proteins of interest were normalized to the total protein loading intensity or to its respective total protein intensity in the same lane after membrane stripping in a buffer containing (62.5 mM Tris-HCl (pH 6.8), 2% SDS and 0.1 M 2-β Mercaptoethanol) for 10 min at 50-60°C with gentle shaking under safety hood and redevelopment.

Antibodies used for Western blots: Primary - mouse anti-AcetyTub, 1:500 (Sigma, T7451); mouse anti-GAPDH, 1:2500 (Santa Cruz sc-32233), mouse anti-PolyGluTub, 1:500 (Sigma T9822); rat anti-tryosinated tubulin (YL1/2), 1:1000 (Abcam ab6160); sheep anti-tubulin (total), 1:1000 (Cytoskeleton ATN02). Secondary - goat anti-mouse IgG HRP, 1:5000 (Dianova 115-035-003); goat anti-rabbit IgG HRP 1:5000 (Dianova 111-035-003); donkey anti-rat IgG HRP, 1:5000 (Dianova DAB-87223); donkey anti-sheep IgG HRP, 1:5000 (Dianova 713-035-147).

TACC3 linear regression analysis

Length of neurites were measured manually using Fiji - ImageJ (NIH). AcetyTub and TACC3 intensity were measured selecting the neurites shaft using the polygon selection. The Max intensity was plotted for each condition. Prism 9 software was used to calculate the correlation between the variables.

TACC3 comets analysis

Epifluorescence time-lapse live-images of tdTomato-TACC3 expressing primary neurons transfected DIV1 rat hippocampal neurons (via Amaxa nucleofection) were used for analysis. The number of TACC3 comets entering each neurite was measured from the time-lapses of stage 2 hippocampal neurons. Lines were drawn along the width of each neurite at its base, to generate kymographs, with a line width of 1, using Fiji - ImageJ. From the kymographs, the number of TACC3 comets (that appear as distinct spots) and the length of respective neurites were manually analyzed. For Pearson correlation analysis, values were normalized according to standard score (*Z* score) and axes are represented in units of standard deviation [σ].

Measurement of stable MTs

Primary mouse cortical neurons were cultured for 48h after plating and then were treated for 30 min with 6 μM nocodazole and fixed as explained above with PFA and Methanol (see Immunofluorescence). The mean intensity value of AcetyTub in the soma was measured using Fiji - ImageJ software as described above.

Neurite length and terminals analysis

Mouse cortical neurons transfected with tDimer together with control, Cep120-shRNA, Cep120-GFP, TACC3-shRNA, SPL-B-treated control cells and SPL-B-treated Cep120-GFP cells were used for neurite length and terminals analysis. For Neurite length analysis, in

each cell total length of all neurites, length of the longest neurite and length of other neurites were measured manually from all the mentioned conditions using the ROI manger in Fiji - ImageJ (NIH). For Neurite terminals analysis, total number of neurite terminals per cell was counted manually from all the above-mentioned conditions.

Cortical cells preparation and FACS sorting

Brain cortices transfected with Cep120 shRNA or controls in combination with pNeuroD-GFP, via IUE at E15, harvested at E19 were prepared as described above. The concentration of shRNA plasmids injected was 4-fold higher than that of the pNeuroD-GFP plasmids. We used 2 μg/μL for shRNA (control or Cep120), 0.5 μg/μL pNeuroD-GFP plasmid. Four days later pregnant mice were anesthetized with CO2/O2, euthanized before taking the E19 embryos out from their uteri. Embryos were then decapitated, skulls were opened, brains were collected in petri dishes with Hibernate™-E medium (Invitrogen) on ice. Hemispheres were separated, meninges were carefully stripped away, and cortices were dissected on ice. Transfected (fluorescent) cortical regions were identified and dissected on ice under a stereo microscope (Olympus SZX16) equipped with a UV light source. The isolated cortical regions were then incubated in 1x HBSS (Invitrogen) containing papain and DNase (Worthington) for 10 min at 37°C neurons, DMEM/10% FCS was added to stop the digestion reaction, then washed with 1x HBSS (warm), which is then replaced with FACS buffer (0.2mM EDTA in Ca-/Mg-free PBS). Cells were then triturated using a fire polished Pasteur pipette with 1mm opening in 2mL FACS buffer for 10-20 times thoroughly but gently until suspended. Cells were then centrifuged at 150g for 10 min in 1 mL cold FACS buffer. Cells were then passed through a 40μm insert filter to remove clusters and filter washed 2 times with 0.5mL FACS buffer. The filtrate was then taken for sorting GFP + cells at the Cytometry & Cell Sorting Core Unit, Stem Cell Transplant Clinic, Oncology Center at the UKE Hamburg, using the BD FACSAria (TM) Fusion Cell Sorter through a 70μm Nozzle at 4°C. Immediately after sorting, cells were collected by centrifugation (150-200xg, 10min, 4°C), after which an excess of FACS buffer is removed in sterile conditions. The cells pelleted were then stored in - 80°C until further use. FAC sorted pNeuroD-GFP cells from cortices of 1 or 2 embryos were pooled for proteome analysis.

Sample preparation for proteome analysis

Ten FACS sorted cell collections were lysed in 100 mM triethyl ammonium bicarbonate (TEAB) and 1% w/v sodium deoxycholate (SDC) buffer, boiled at 95°C for 5 min and sonicated with a probe sonicator. Disulfide bonds were reduced with dithiothreitol (DTT), alkylated in presence of iodoacetamide (IAA) and digested with trypsin (sequencing grade, Promega) at 37°C overnight. SDC was precipitated by the addition of 1% v/v formic acid (FA) followed by centrifuged at 16,000 g and the supernatant was transferred into a new tube. Samples were dried in a vacuum centrifuge. Afterwards, samples were resuspended in 100 mM TEAB and labelled with TMT10plex™ (Thermo Scientific; Cat# 90110) according to the manufacture's instruction, except a 1/10 downscaling was used for labeling low amounts of proteins. After quenching of TMT labeling with hydroxyl amine, the nine samples were combined based on similar cell numbers and dried again in a vacuum centrifuge.

About 1μg each of the TMT labeled samples were resuspended in 10 mM ammonium bicarbonate (pH = 8.5) for basic reversed phase chromatography. Peptides were separated within a 25 min gradient (3–35% acetonitrile) on a monolith column (ProSwift™ RP-4H, 1 mm × 250 mm, Thermo Fisher Scientific) using an HPLC system (Agilent 1200 series, Agilent Technologies) with a two-buffer system. Equilibration buffer: 10 mM ammonium bicarbonate (pH = 8.5), elution buffer 10 mM ammonium bicarbonate in 90% acetonitrile. A fraction collector was used to collect 1 min fractions which were then combined to 13 fractions and dried in a vacuum centrifuge.

Analysis of the TMT-labeled tryptic peptides with liquid chromatography coupled to tandem mass spectrometry (LC-MS/MS)

TMT-labeled tryptic peptides were resuspended in 0.1% formic acid. NanoLC chromatographic separation was achieved on an UPLC system (Dionex Ultimate 3000, Thermo Fisher Scientific). Attached to the UPLC was a C18 reversed phase peptide (RP) trap (Acclaim PepMap 100, 100 μm × 2 cm, 100 Å pore size, 5 μm particle size) for desalting a purification followed by a C18 RP analytical column (Acclaim PepMap 100, 75 μm × 50 cm, 100 Å pore size, 2 μm particle size). Peptides were separation using a 60 min gradient with increasing ACN concentration from 2%–30% ACN. The eluting peptides were analyzed on a quadrupole, orbitrap, ion trap tribrid mass spectrometer (Fusion, Thermo Fisher Scientific) in data dependent acquisition (DDA) mode with synchronous precursor selection MS^3 (SPS-MS^3 (McAlister et al., 2014)). Therefore, the topmost intense ions per precursor scan (2×10^5 ions, 120,000 Resolution, 120 ms fill time) were analyzed first by MS/MS in the ion trap (CID at 35 normalized collision energy, 1×10^4 ions, 50 ms fill time) in a range of 400–1200 m/z and spectra demonstrating TMT reporter ions were further analyzed by synchronous precursor selection from the MS/MS spectrum (max. 10) and in the Orbitrap (HCD 65 normalized collision energy, 5×10^4 ions, 50.000 resolution, 86 msec fill time). A dynamic precursor exclusion of 30 s was used.

LC-MS/MS data analysis and processing

Acquired LC-MS/MS data were searched against the mouse (release April 2020, 17,013 protein entries) protein database downloaded from https://www.uniprot.org/ (EMBL) using the Sequest algorithm integrated in the Proteome Discoverer software version 2.4 (Thermo Fisher Scientific. Mass tolerances for precursors was set to 10 ppm and 0.6 Da for fragments. Carbamidomethylation on cysteine residues and TMT label modification on the peptide N-terminus and the amine group in the lysine sidechain were set as a

fixed modification and the oxidation of methionine, pyro-glutamate formation at glutamine residues at the peptide N-terminus as well as acetylation of the protein N-terminus, methionine loss at the protein N-terminus and the acetylation after methionine loss at the protein N-terminus were allowed as variable modifications. Only peptides with a high confidence (false discovery rate <1% using a decoy database approach) were accepted as identified. TMT reporter areas were extracted from corresponding MS^3 spectra for each identified peptide and to generate relative protein abundance level across all the 10 samples.

Out of the 10 samples (5x Controls and 5x Cep 120shRNA) used for TMT-labelling, one of the controls samples (TMT9) that had low number of FAC sorted GFP + cells in comparison to the other samples showed high variability for many proteins, hence excluded from the statistical analysis. The least cell number was 12164 GFP + cells, as estimated by cell sorter, for the rest of the 9 samples (4 x controls and 5 x Cep120 shRNA) used for further analysis.

Bioinformatic analysis of proteome data

Out of the 1093 proteins quantified, 186 are significantly altered in control vs Cep120sh groups, with $p < 0.05$ (See Table S1. LC-MSMS Rawdata.xlsx for details). For heatmap, a hierarchical clustering of the 50 proteins with the lowest significant p-value (<0.05) that identifies a relative down regulation of protein expression in Cep120 shRNA neurons in comparison with the controls from normalized data as stated in the Raw data (See Table S1. LC-MSMS Rawdata.xlsx for details). The dendrogram represents the hierarchical clustering with a distance score based on Pearson-correlation coefficients (*Z* score −2 to 2) and a complete linkage clustering as cluster agglomeration criteria ((dis-) similarity between group Cep120 versus Control). Pathway diagrams shown in Figure 5D is modified and reproduced from: Wiki pathways: https://www.wikipathways.org/index.php/Pathway:WP2038; Cell Signaling Technology Pathways: https://www.cellsignal.de/contents/science-cst-pathways-adhesion-ecm-cytoskeleton/regulation-of-MT-dynamics/pathways-micro.

For the STRING analysis, the proteins whose levels were found to be significantly different between the two conditions (See Table S3. LC-MSMS STRING.xlsx for details)., were used STRING v11 (Szklarczyk et al., 2019), allowing to predict functional associations between proteins (von Mering et al., 2003).

Gene set enrichment analysis (GSEA) was performed with WebGestalt (Liao et al., 2019). Briefly all the proteins that were quantified in each of the replicates (n = 1093) were ordered by their relative difference between the two conditions and analyzed with WebGestalt for the three non-redundant functional gene ontology databases (biological process, cellular component, molecular function). All the advanced parameters were kept as indicated in the presets (for details refer to http://www.webgestalt.org/) (See Table S2. LC-MSMS GSEA.xlsx for details).

Image processing

Linear adjustment of brightness and contrast was performed on images using Photoshop CS or Fiji - ImageJ.

QUANTIFICATION AND STATISTICAL ANALYSIS

Statistical analysis was performed using the GraphPad Prism software versions 8 and 9. The Student's t-test (two-tailed) was used to compare means of two groups, whereas analysis of variance (ANOVA) was used when comparing more than two groups. Asterisks *, **, *** and **** represent $p < 0.05$, 0.01, 0.001, and 0.0001, respectively. Error bars in the graphs always represent standard error of mean. Pearson correlation analysis was performed for showing a linear relationship between two sets of data. Below are the statistical details for the data shown in main figures.

Figure 1B. Mean ± SEM values for stage 1 (n = 4 neurons) = 1.000 ± 0.05822, stage 2 (n = 4 neurons) = 1.326 ± 0.03554, and stage 3 (n = 5 neurons) = 1.280 ± 0.01901. p = 0.0002 by one-way ANOVA, post hoc Tukey's test, ***p = 0.0003 for stage 1 vs. stage 2; ***p = 0.0009 for stage 1 vs. stage 3.

Figure 1D. Mean ± SEM values for stage 1 (n = 4 neurons) = 1.000 ± 0.05139, stage 2 (n = 3 neurons) = 1.338 ± 0.07022, and stage 3 (n = 3 neurons) = 1.314 ± 0.02403. p = 0.0037 by one-way ANOVA, post hoc Tukey's test, **p = 0.0061 for stage 1 vs. stage 2; **p = 0.0090 for stage 1 vs. stage 3.

Figure 1E. Quantifications show the area of Tubulin PTMs -

AcetyTub: Mean ± SEM values for stage 1 neurons = 1.000 ± 0.09164, stage 2 neurons = 2.141 ± 0.1909, stage 3 neurons = 2.363 ± 0.1182. p < 0.0001 by one-way ANOVA, post hoc Tukey's test, ****p < 0.0001; n = 8 cells per each stage.

TyrTub: Mean ± SEM values for stage 1 neurons = 1.000 ± 0.06577, stage 2 neurons = 1.453 ± 0.1147, stage 3 neurons = 1.676 ± 0.1042. p = 0.0003 by one-way ANOVA, post hoc Tukey's test, ***p = 0.0002, *p = 0.0132; n = 8 cells each (stage 1, stage 2) and 10 cells (stage 3).

PolyGluTub: Mean ± SEM values for stage 1 neurons = 1.000 ± 0.08415, stage 2 neurons = 1.166 ± 0.1324, stage 3 neurons = 1.491 ± 0.1364. p = 0.0254 by one-way ANOVA, post hoc Tukey's test, *p = 0.0223; n = 7 cells (stage 1), 6 cells (stage 2) and 8 cells (stage 3).

α-tubulin: Mean ± SEM values for stage 1 neurons = 1.000 ± 0.1288, stage 2 neurons = 1.474 ± 0.2105, stage 3 neurons = 1.620 ± 0.1116. p = 0.0260 by one-way ANOVA, post hoc Tukey's test, *p = 0.0279; n = 7 cells (stage 1), 6 cells (stage 2) and 6 cells (stage 3).

Figure 2B.

Left panel: Mean ± SEM values of median speed from stage 1 = 0.2168 ± 0.01073, stage 2 = 0.2496 ± 0.01101, stage 3 = 0.1854 ± 0.01829. p = 0.0190 by one-way ANOVA, post hoc Tukey's test, *p = 0.0152. For stage 1 vs stage 2: #p = 0.0654 by unpaired Student's t-test.

Middle panel: Mean ± SEM values of the characteristic growth (λ) per each frame for stage 1 = 0.6805 ± 0.04982, stage 2 = 0.9314 ± 0.05477, stage 3 = 0.5967 ± 0.08114. p = 0.0065 by one-way ANOVA, post hoc Tukey's test, *p = 0.0285, **p = 0.0075.

Right panel: Mean ± SEM values of growth half lifetime (τ) obtained from stage 1 = 2.835 ± 0.3180, stage 2 = 3.292 ± 0.9624, stage 3 = 3.796 ± 0.3562. p = 0.6124 by one-way ANOVA, post hoc Tukey's test.

For data shown in Figures 2B and 2C.

EB3 tracks (for speed and duration) analyzed per cell in the respective stages are as follows:

stage 1 (n = 5): cell 1 = 807; cell 2 = 935; cell 3 = 971; cell 4 = 1166; cell 5 = 885. stage 2 (n = 5): cell 1 = 1174; cell 2 = 462; cell 3 = 363; cell 4 = 498; cell 5 = 855.

stage 3 (n = 4): cell 1 = 2028; cell 2 = 470; cell 3 = 1249; cell 4 = 663.

EB3 comets (for displacement) analyzed per cell in the respective stages are as follows:

stage 1 (n = 5): cell 1 = 2461; cell 2 = 2211; cell 3 = 2380; cell 4 = 4576; cell 5 = 4125. stage 2 (n = 5): cell 1 = 2409; cell 2 = 1098; cell 3 = 652; cell 4 = 3023; cell 5 = 4169. stage 3 (n = 4): cell 1 = 8823; cell 2 = 1464; cell 3 = 4122; cell 4 = 3474.

Figure 3C. DMSO treated stage 1 cells (n = 40) with 1 axon = 90%, more than 1 axon = 10%, CytoD treated stage 1 cells (n = 36) with 1 axon = 86.11%, more than 1 axon = 13.89%, Taxol treated stage 1 cells (n = 20) with 1 axon = 35%, more than 1 axon = 65%. DMSO treated stage 2 cells (n = 19) with 1 axon = 94.74%, more than 1 axon = 5.26%, CytoD treated stage 2 cells (n = 20) with 1 axon = 25%, more than 1 axon = 75%, Taxol treated stage 2 cells (n = 10) with 1 axon = 10%, more than 1 axon = 90%.

Figure 3E. Acetylated to TyrTub ratio (Left): Mean ± SEM values of Control cells = 1.001 ± 0.03024, CytoD treated cells = 1.003 ± 0.04580, Taxol treated cells = 2.129 ± 0.0940. p < 0.0001 by one-way ANOVA, post hoc Tukey's test, ****p < 0.0001. n = 18 in Control, 19 in CytoD and 17 in Taxol groups. Acetylated to α-tubulin ratio (Right): Mean ± SEM values of Control cells = 0.9996 ± 0.05200, CytoD treated cells = 0.9985 ± 0.02648, Taxol treated cells = 1.287 ± 0.03621. p < 0.0001 by one-way ANOVA, post hoc Tukey's test, ****p < 0.0001. n = 14 in Control, 19 in CytoD and 19 in Taxol groups.

Figure 3G. *p = 0.0489 by unpaired Student's t-test. Cell lysates are obtained from three different experiments.

Figure 4B. Mean ± SEM values of Cep120 shRNA cells (n = 20) = 0.6322 ± 0.0678, control cells (n = 27) = 1.000 ± 0.0676 and Cep120-GFP cells (n = 31) = 1.249 ± 0.0641. p < 0.0001 by one-way ANOVA, post hoc Tukey's test, **p = 0.0014, *p = 0.0194.

Figure 4D. Mean ± SEM values for length of all neurites in, Cep120 shRNA neurons (n = 60) = 220.4 ± 12.14, control neurons (n = 93) = 441.1 ± 16.62, Cep120-GFP neurons (n = 51) = 444.4 ± 20.25. Mean ± SEM values for length of longest neurite in Cep120 shRNA cells = 111.4 ± 6.56, control neurons = 257.1 ± 14.65, Cep120-GFP cells = 188.2 ± 12.67. Mean ± SEM values for length of other neurites in Cep120 shRNA cells = 109 ± 9.062, control neurons = 186.9 ± 10.46, Cep120-GFP cells = 256.2 ± 13.36. p < 0.0001 by one-way ANOVA, post hoc Tukey's test, ****p < 0.0001, **p = 0.011.

Figure 4E. Mean ± SEM values for neurite terminal per cell in Cep120 shRNA neurons (n = 60) = 9.517 ± 0.6127, control neurons (n = 93) = 14.66 ± 0.5752, Cep120-GFP neurons (n = 51) = 15.16 ± 0.8643. p < 0.0001 by one-way ANOVA test, post hoc Tukey's test, ****p < 0.0001.

Figure 4F. Mean ± SEM values for percentage of Cep120 shRNA cells (n = 258) with no axon = 69.90 ± 2,450, 1 axon = 29.43 ± 2.404, more than 1 axon = 0.7000 ± 0.3606; percentage of control cells (n = 364) with no axon = 13.01 ± 3.762, 1 axon = 79.10 ± 3.785, more than 1 axon = 7.892 ± 1.677; percentage of Cep120-GFP neurons (n = 172) with no axon = 19.01 ± 4.226, 1 axon = 40.30 ± 5.231, more than 1 axon = 40.44 ± 1.279. α = 0.05 by two-way ANOVA, post hoc Tukey's test, ****p < 0.0001.

Figures 4B, 4D, 4E and 4F, data is obtained from cortical cultures of 3 or more IUE embryos from at least 2 different mothers.

Figure 4H. Mean ± SEM values of leading process width in Cep120 shRNA cells = 2.501 ± 0.1199, controls = 2.385 ± 0.1031, Cep120-GFP cells = 2.976 ± 0.2061. p = 0.0204 by one-way ANOVA, post hoc Tukey's test, *p = 0.0155.

Figure 4I. Mean ± SEM values of length to width ratio of soma in Cep120 shRNA cells = 1.852 ± 0.0664, control cells = 2.148 ± 0.0927, Cep120-GFP cells = 2.485 ± 0.1683. p = 0.0002 by one-way ANOVA, post hoc Tukey's test, ***p = 0.0002, *p = 0.0344.

Figure 4K. Mean ± SEM values for all neurites in Cep120 shRNA cells = 1.463 ± 0.0906, control cells = 2.077 ± 0.0505, Cep120-GFP cells = 3.296 ± 0.1984. Mean ± SEM values for apical neurites in Cep120 shRNA cells = 0.8500 ± 0.0440, control neurons = 1.031 ± 0.0216, Cep120-GFP cells = 1.407 ± 0.0964. Mean ± SEM values for basal neurites in control neurons = 1.000 ± 0.0310, Cep120 shRNA cells = 0.5750 ± 0.0610, Cep120-GFP cells = 1.444 ± 0.1233. Mean ± SEM values for lateral neurites in Cep120 shRNA cells = 0.0375 ± 0.0278, control cells = 0.0461 ± 0.0262, Cep120-GFP cells = 0.4444 ± 0.1541. p < 0.0001 by Kruskal-Wallis ANOVA test, post hoc Dunn's test, ****p < 0.0001. *p = 0.0112, n.s. = not significant.

Data shown in Figure 4 H, I and K is obtained from Cep120 shRNA neurons (n = 59), control neurons (n = 67) and Cep120-GFP neurons (n = 27) three E19 mouse brains slices from two Cep120-GFP and three control and three Cep120 shRNA embryonic mouse brains.

Figure 6 C, 6D and 6G, data is obtained from n = 10 cells per experiment obtained from 2 (6 C, 6D) or 3 (6G) different rat cultures.

Figure 7B. Total tubulin: Mean ± SEM values for the soma of control neurons (n = 29) = 1.000 ± 0.06912, SPL-B neurons (n = 24) = 0.9243 ± 0.07903, and Cep120-GFP + SPL-B neurons (n = 18) = 1.157 ± 0.09303. p = 0.1532 by one-way ANOVA. AcetyTub: Mean ± SEM values for the soma of control neurons (n = 16) = 1.000 ± 0.1029, SPL-B neurons (n = 15) = 0.3778 ± 0.0325, and Cep120-GFP + SPL-B neurons (n = 12) = 0.6836 ± 0.0758. p < 0.0001 by one-way ANOVA, post hoc Tukey's test, ****p < 0.0001, *p < 0.05. Poly-GluTub: Mean ± SEM values for the soma of control (n = 35) cells = 1.000 ± 0.07915, SPL-B cells = 0.3121 ± 0.03632, and Cep120-GFP + SPL-B cells = 0.3227 ± 0.05454. p < 0.0001 by one-way ANOVA, post hoc Tukey's test, ****p < 0.0001.

Figure 7D. Mean ± SEM values for length of all neurites of control cells (n = 48) = 292.2 ± 15.06, SPL-B cells (n = 45) = 68.20 ± 8.768, and Cep120-GFP + SPL-B cells (n = 40) = 131.4 ± 13.60. Mean ± SEM values for length of longest neurite in control cells = 148.7 ± 10.96, SPL-B cells = 44.57 ± 5.252, Cep120-GFP cells = 81.89 ± 9.284. Mean ± SEM values for length of other neurites in control cells = 143.5 ± 10.01, SPL-B cells = 23.63 ± 4.889, and Cep120-GFP + SPL-B cells = 49.47 ± 7.975. $p < 0.0001$ by one-way ANOVA, post hoc Tukey's test, ****$p < 0.0001$, **$p = 0.0026$, *$p = 0.0126$, n.s. = not significant.

Figure 7E. Mean ± SEM values for neurite terminal per cell for controls (n = 48) = 10.23 ± 0.7313, SPL-B cells (n = 45) = 2.733 ± 0.2551, and Cep120-GFP + SPL-B cells (n = 40) = 3.950 ± 0.4370. $p < 0.0001$ by one-way ANOVA, post hoc Tukey's test, ****$p < 0.0001$, n.s. = not significant.

Figure 7F. Mean ± SEM values for percentage of control cells (n = 123) with no axon = 30.57 ± 12.71, 1 axon = 66.01 ± 10.79, more than 1 axon = 3.425 ± 1.935; percentage of SPL-B cells (n = 106) with no axon = 86.83 ± 6.500, 1 axon = 13.17 ± 6.500, more than 1 axon = 0.000 ± 0.000; percentage of SPL-B treated with Cep120-GFP cells (n = 56) with no axon = 61.99 ± 6.430, 1 axon = 38.01 ± 6.430, more than 1 axon = 0.000 ± 0.000. $\alpha = 0.05$ two-way ANOVA, post hoc Tukey's test, ****$p < 0.0001$, **$p = 0.0013$. Data shown in Figure 7 B, D, E and F is obtained from cortical cultures of 3 or more IUE embryos from at least 2 different mothers.